

XMM-NEWTON OBSERVATIONS OF THE M31 NORTHERN DISK: PROPERTIES OF SELECTED X-RAY SOURCES AND DIFFUSE EMISSION.

SERGEY TRUDOLYUBOV^{1,2,3}, OLEG KOTOV^{2,4}, WILLIAM PRIEDHORSKY², FRANCE CORDOVA¹, AND
KEITH MASON⁵

Draft version November 1, 2018

ABSTRACT

We present the results of XMM-Newton survey of the northern part of the disk of M31. The results of a spectral and timing analysis of the thirty seven brightest sources are presented. Combining the results of X-ray analysis with available data at other wavelengths, we were able to classify $\sim 50\%$, or 19 out of 37 sources.

Two sources in our sample were previously unknown: the hard X-ray source XMMU J004415.8+413057 and a transient supersoft source XMMU J004414.1+412206. We report the discovery of possible X-ray pulsations from the source XMMU J004415.8+413057 with a period of 197 s. The spectral and timing properties of XMMU J004415.8+413057 make it first accreting X-ray pulsar candidate detected in M31.

We found six X-ray sources to be coincident with M31 globular cluster (GC) candidates. The spectral properties of GC sources were found to be similar to that of the bright Galactic low mass X-ray binaries located in the bulge and globular clusters. The comparison of the X-ray properties of GC sources with optical properties of their host globular clusters has shown that the brightest sources with luminosity, L_X above $\sim 10^{38}$ ergs s⁻¹ tend to reside in more metal poor clusters.

Three X-ray sources were identified with SNR based on their X-ray spectra and positional coincidence with SNR candidates from optical and radio surveys. We found five bright X-ray sources to coincide with Galactic foreground stars. Two of them demonstrate a remarkable variability of X-ray flux on a time scale of individual *XMM-Newton* observations. Two X-ray sources coincide with radio sources and are probably distant radio galaxies/AGN.

The properties of the remaining 18 bright X-ray sources detected in our survey are consistent with AGN in the background of M31 and X-ray binaries belonging to M31. Many of them show high values of low-energy absorption, which combined with extreme faintness of their possible optical counterparts makes them an obscured AGN candidates.

We report on the first unambiguous detection of the soft unresolved X-ray emission from the disk of M31. The unresolved emission follows the pattern of the spiral arms and can be traced up to distance of $\sim 0.5^\circ$ (~ 7 kpc at 760 kpc) from the center of the galaxy. The spectrum of the unresolved emission shows dominant soft thermal component which can be fitted with a ~ 0.3 keV optically thin thermal plasma emission models. We suggest that significant part of this diffuse soft X-ray component may represent hot diffuse gas in the spiral arms of M31 and emission from normal stars in the disk of M31.

Subject headings: galaxies: individual (M31) — X-rays: galaxies — X-rays: stars

1. INTRODUCTION

The Andromeda Galaxy (M31), the closest spiral galaxy to our own (760 kpc; van der Bergh 2000), is a unique object for the study of X-ray astronomy. M31 is in many respects similar to the Milky Way and even called its “twin sister”. M31 hosts hundreds of X-ray sources, which are observed at a nearly uniform distance, and due to the favorable orientation of the M31, they are less obscured by interstellar gas and dust than those in the Galaxy. M31 was observed extensively with *Einstein*, *ROSAT*, *Chandra* and *XMM-Newton* missions, detected hundreds of X-ray sources, identified with different types of X-ray emitting objects (Trinchieri & Fabbiano 1991; Primini et al. 1993; Supper et al. 1997, 2001; Kong et al. 2002; Shirey et

al. 2001). Although the central part of M31 was subject to deep X-ray surveys, the outer disk of the galaxy was covered by observations with relatively low sensitivity (Williams et al. 2003).

In this paper we present the results from the deep *XMM-Newton* observations of the northern parts of the disk of M31. We concentrate on the spectral and timing analysis of a selected sample of 37 bright X-ray sources. We also report on the first unambiguous detection of the diffuse X-ray emission associated with disk of M31.

2. OBSERVATIONS AND DATA ANALYSIS

Three regions of the northern part of galactic disk of M31 were observed with *XMM-Newton* on January 5 (Obs. #1)(Trudolyubov et al. 2002a), January 26 (Obs. #2),

¹University of California, Riverside, CA 92507

²Los Alamos National Laboratory, Los Alamos, NM 87545

³Space Research Institute, Russian Academy of Sciences, Profsoyuznaya 84/32, Moscow, 117810 Russia

⁴Harvard-Smithsonian Center for Astrophysics, Cambridge, MA

⁵Mullard Space Science Laboratory, University College London, UK

and June 29, 2002 (Obs. #3) as a part of the Guaranteed Time Program (PI: K. O. Mason) (Table 1, Figure 1). The 2002, January 6 *XMM-Newton* observation of the central part of M31 (Trudolyubov et al. 2002b) (Obs. #4) provides additional coverage of the inner disk. In the following analysis we use the data from three European Photon Imaging Camera (EPIC) instruments: two EPIC MOS detectors (Turner et al. 2001) and the EPIC-pn detector (Strueder et al. 2001). In the first three observations EPIC instruments were operated in the *full window* mode (30' FOV) with the *medium* optical blocking filter. In the Obs. #4 a combination of the *full window* mode and *thin* optical blocking filter was used.

We reduced EPIC data with the *XMM-Newton* Science Analysis System (SAS v 5.3) ⁶. We performed standard screening of the EPIC data to exclude time intervals with high background levels.

Images in celestial coordinates with a pixel size of 2'' have been accumulated in the 0.3 – 1.0, 1.0 – 2.0, 2.0 – 7.0 and 0.3 – 7.0 keV energy bands for the EPIC-MOS1, MOS2 and pn detectors. We produced a three-color image of the northern disk regions of M31 combining the images in the 0.3 – 1.0 (soft), 1.0 – 2.0 (medium) and 2.0 – 7.0 keV (hard) energy bands and using red, green and blue color scales to represent the X-ray intensities in these bands (Fig. 1). The spectral energy distribution of the source defines its color in this image. The sources with soft X-ray spectra (i.e. supersoft sources, thermal supernova remnants and Galactic foreground stars) appear in red, while sources with hard spectra are blue.

X-ray sources were detected with program based on a wavelet decomposition algorithm, set at a 4σ threshold. For our current analysis, we expect error in the source position determination to be dominated by residual systematic error of the order 2 – 5''. We corrected the count rates of the sources for the vignetting of the XMM telescope, based on the Current Calibration Files provided with SAS.

We studied the spectral and timing properties of all X-ray sources in our sample. Each source in our sample provided between 300 and 18000 counts in EPIC detectors allowing high quality spectroscopic and timing analysis.

To generate lightcurves and spectra of X-ray sources, we used elliptical extraction regions with semi-axes size of $\sim 20 - 80''$ (depending on the distance of the source from the telescope axis) and subtracted as background the spectrum of adjacent source-free regions with subsequent normalization by a ratio of the detector areas. We used data in the 0.3 – 10 keV energy band because of the uncertainties in the calibration of the EPIC instruments outside this range. All fluxes and luminosities derived from spectral analysis apply to this band, unless specified otherwise. For the sources with soft (Galactic foreground stars, SNR candidates) and supersoft X-ray spectra we considered only the 0.3 – 3.0 and 0.2 – 1.0 keV spectral ranges, since their flux was negligible above 3.0 and 1.0 keV respectively. We used spectral response files generated by XMM SAS tasks. Spectra were grouped to contain a minimum

of 20 counts per spectral bin in order to allow χ^2 statistics and fit to analytic models using the XSPEC v.11⁷ fitting package (Arnaud 1996). EPIC-pn, MOS1 and MOS2 data were fitted simultaneously, but with normalizations varying independently.

Fourier power density spectra (PDS) were produced using the lightcurves in the 0.3 – 7.0 keV energy band. Then we performed folding analysis in the vicinity of the frequency peaks identified from PDS. We used standard XANADU/XRONOS v.5 ⁸ tasks to perform analysis of the timing properties of bright X-ray sources.

In the following analysis we assume a source distance of 760 kpc (van den Bergh 2000).

3. SELECTED X-RAY SOURCES: IDENTIFICATION AND CLASSIFICATION

Using the procedure described above, we detected about 300 X-ray point sources in the three *XMM* M31 northern disk fields. The complete X-ray source catalog will be presented in a follow-up paper. Here we study a sample of 37 sources selected on the basis of their brightness; each individual source was required to have more than 300 counts in the EPIC. The information on the positions and identifications of the selected X-ray sources is shown in Table 2. The X-ray images of the northern disk regions of M31 with source positions marked are shown in Fig. 2.

We searched for optical, infrared and radio counterparts to the bright XMM sources in the northern disk of M31 using the existing catalogs and images from the CTIO/KPNO Local Group Survey (LGS) (Massey et al. 2001) and the Second Generation Digitized Sky Survey. We varied the search radius based on both the accuracy of the catalogs and localization errors of *XMM* sources (upper limit of 5''). We used the following catalogs and corresponding search radii:

- i) *X-ray sources*: the *ROSAT*/PSPC catalog of sources in the field of M31 (Supper et al. 1997, 2001) (SHP97,SHP01) – search radius specified by position accuracy for each individual source. All but five bright *XMM* sources were detected in the *ROSAT*/PSPC survey of M31 (Table 2).
- ii) *Globular cluster candidates*: the Bologna catalog (Battistini et al. 1987), the catalog by Magnier (1994), and the HST globular cluster candidate catalog (Barmby & Huchra 2001) – with search radius of 5''.
- iii) *Supernova remnant candidates*: the lists by Braun & Walterbos (1993) and Magnier et al. (1995) – 10'' search radius.
- iv) *Stellar objects (Galactic foreground stars/background AGN)*: the catalogs of stellar objects by Magnier et al. (1992) and Haiman et al. (1994) and SIMBAD – 3'' search radius.
- v) *Radio sources*: VLA All-sky Survey Catalog ⁹ (Condon et al. 1998)– 5'' search radius.

Inspection of optical images to search for uncatalogued bright star-like objects revealed no additional foreground star candidates. X-ray source #33, however, is very likely a background galaxy based on the shape of its counterparts

⁶See <http://xmm.vilspa.esa.es/user>

⁷<http://heasarc.gsfc.nasa.gov/docs/xanadu/xspec/index.html>

⁸<http://heasarc.gsfc.nasa.gov/docs/xanadu/xronos/xronos.html>

⁹<http://www.cv.nrao.edu/nvss/>

in the LGS and DSS images.

4. BRIGHT X-RAY SOURCES DISCOVERED WITH XMM-NEWTON

4.1. X-ray pulsar candidate XMMU J004415.8+413057

The X-ray source XMMU J004415.8+413057 was discovered with *XMM-Newton* in the 2002 January 5 observation (Trudolyubov et al. 2002a). As the source falls into a CCD gap in both EPIC-MOS detectors, we present the analysis of the source properties based on the EPIC-pn data alone. The spectrum of XMMU J004415.8+413057 is remarkably hard and heavily absorbed at low energies (Fig. 3). The analytic approximation of the spectrum with an absorbed simple power law model gives a photon index of 1.4 and requires an absorbing column of $1.3 \times 10^{22} \text{ cm}^{-2}$ (Table 3; Fig. 3). The corresponding absorbed 0.3 – 10 keV luminosity of the source was $\sim 9 \times 10^{36} \text{ ergs s}^{-1}$.

The X-ray source XMMU J004415.8+413057 shows a significant variability on a time scales of several years. It was not detected in the previous observations with *Einstein* and *ROSAT*. Using the data of archival 1996, July 7 deep *ROSAT*/HRC observation, and assuming the same spectral shape as measured with *XMM*, we estimate a 2σ upper limit to the source luminosity of $\sim 2 \times 10^{36} \text{ ergs s}^{-1}$. This implies that XMMU J004415.8+413057 was at least a factor of 4 fainter during *ROSAT* observation in July 1996.

The analysis of the timing properties of XMMU J004415.8+413057 revealed probable coherent pulsations of the X-ray flux with a period of 197.19(5) s (Fig. 4a,b). We estimated statistical significance of the corresponding peak in the source PDS. The probability that any one of the 1300 frequency bins in the PDS would have a noise value exceeding the power level of this peak is $\sim 1\%$ (Vaughan et al. 1994). Figure 4d shows EPIC-pn light curve of XMMU J004415.8+413057 folded on the 197.19 s best period of the pulsation. The pulse profile shows a nearly sinusoidal form with $\sim 40\%$ flux modulation.

Another feature of the source PDS is a group of frequency peaks corresponding to the ~ 5900 s slow modulation (Fig. 4a,c). Figure 4e shows EPIC-pn light curve of XMMU J004415.8+413057 folded on the 5900 s period of this modulation.

In order to investigate the energy dependence of the 197-s pulsations, we constructed light curves in the 0.3 – 2.0 and 2.0 – 7.0 keV energy bands folded on the best period (Fig. 5). The energy-resolved pulse profiles show marginal differences between the soft and hard energies with excess of the hard emission at phase ~ 0.15 .

Together with the X-ray spectrum, probable 197-s pulsations strongly support the identification of XMMU J004415.8+413057 as a first accreting pulsar candidate in M31 and possible HMXB. The extreme level of low energy absorption in the spectrum (at least 10 times Galactic foreground value) could be consistent with absorption within HMXB system or source location in the region with high density of the neutral gas (e.g. molecular cloud). The 5900-s modulation of the X-ray flux could be manifestation of some instability time scale of the accretion flow in this system. A significant variability of the the source on a time scales of several years could imply possible transient/recurrent nature of the source.

4.2. Supersoft X-ray transient XMMU J004414.1+412206

The supersoft X-ray transient source XMMU J004414.1+412206 was discovered on 2002 January 5 using *XMM* (Trudolyubov et al. 2002a). The *XMM* discovery was confirmed by detection of the source with *Chandra* during Jan. 8 and 16, 2002 observations (Garcia et al. 2002). The search for the optical counterparts did not yield any object brighter than $m_v \sim 20$ within *XMM* and *Chandra* source error boxes. The X-ray luminosity of XMMU J004414.1+412206 declined from $\sim 8 \times 10^{36} \text{ ergs s}^{-1}$ on Jan. 5 to $\sim 5 \times 10^{36} \text{ ergs s}^{-1}$ on Jan. 8 (Garcia et al. 2002) for an assumed distance of 760 kpc. The energy spectra of the source obtained with *XMM-Newton*/EPIC-MOS1 and MOS2 detectors on January 5 are shown in Figure 3. The approximation of the EPIC-MOS spectra with the absorbed blackbody radiation model gives a characteristic temperature of $\sim 34 \text{ eV}$ and a relatively high absorbing column of $\sim 4 \times 10^{21} \text{ cm}^{-2}$ (Table 3; Figure 3).

The energy spectrum of XMMU J004414.1+412206 is typical for a supersoft X-ray sources, AM Her systems, isolated white dwarfs and X-ray dim neutron stars. Its luminosity of $\sim 8 \times 10^{36} \text{ ergs s}^{-1}$ for a distance of 760 kpc is too high to originate from an AM Her system in M31 (Ramsay et al. 1994). On the other hand, the transient behavior of the object poses a serious problem for a foreground isolated white dwarf or a neutron star identification. The absence of the bright optical objects in the error box of XMMU J004414.1+412206 excludes an explanation as an AM Her system located within our Galaxy.

The remaining possibility is that XMMU J004414.1+412206 is similar to the Galactic supersoft sources. Then its X-ray emission may be interpreted as a result of thermonuclear burning of the accreted matter on the surface of the white dwarf (see Kahabka & van den Heuvel 1997 for a review). The transient behavior of the source hints that it may be a classical Nova in the supersoft X-ray spectral phase, several tens of days after the peak of the outburst (Kahabka & van den Heuvel 1997). The X-ray source XMMU J004414.1+412206 is the fourth bright supersoft transient detected in M31.

5. GLOBULAR CLUSTER CANDIDATES

The positions of six bright X-ray sources are consistent with globular cluster candidates in M31 (Table 2). We performed a detailed study of their spectral and temporal properties using the data of *XMM-Newton* observations.

5.1. Spectral properties

The spectra of globular cluster candidates were fitted with a variety of spectral models using XSPEC v11. The results of fitting these models to the source spectra are given in Table 4. The spectra of all these objects are relatively hard (Fig. 6) and can be generally described by an absorbed simple power law model with photon index of $\sim 0.8 - 1.9$ and an equivalent absorbing column of $\sim (0.4 - 2.6) \times 10^{21} \text{ cm}^{-2}$ (Table 4). The corresponding isotropic luminosities of the XMM globular cluster sources differ by almost two orders of magnitude and fall between 3.7×10^{36} and $3.3 \times 10^{38} \text{ ergs s}^{-1}$ in the 0.3 – 10 keV energy band, assuming a distance of 760 kpc. The Galactic hydrogen column in the direction of M31 is about $\sim 7 \times 10^{20}$

cm⁻² (Dickey & Lockman 1990); thus within measurement errors our results are consistent with additional absorption due to the interstellar matter in M31 and within the system.

For the three bright sources with luminosities above $\sim 5 \times 10^{37}$ ergs s⁻¹, XMMU J004251.9+413107, XMMU J004301.4+413017 and XMMU J004627.0+420151 models with quasi-exponential cut-off at $\sim 4 - 8$ keV describe the energy spectra significantly better than a simple power law (Table 4; Fig. 6). We used a power law with exponential cut-off and Comptonization models to approximate the spectra of these sources (Table 4).

For the Comptonization model approximation, we used the XSPEC model COMPTT (Sunyaev & Titarchuk 1980, Titarchuk 1994, Titarchuk & Lyubarskij 1995). This model includes a self-consistent calculation of the spectrum produced by the Comptonization of the soft photons in a hot plasma. It contains as free parameters the temperature of the Comptonizing electrons, kT_e , the plasma optical depth with respect to the electron scattering, τ and the temperature of the input Wien soft photon distribution, kT_0 . A spherical geometry was assumed for the Comptonizing region.

The spectra of many luminous Galactic LMXB are well fit with a two component model consisting of a black body-like component which might represent emission from an optically thick accretion disk or from the neutron star surface, together with a Comptonized component which may be interpreted as emission from a hot inner disk region or a boundary layer between the disk and a neutron star. We used such a two-component model to approximate spectra of the brightest globular cluster source, XMMU J004251.9+413107. For the soft component we used disk-blackbody component (Mitsuda et al. 1984). This model has two parameters, the effective radius, $r_{in}\sqrt{\cos i}$, where r_{in} is the inner radius of the disk, i is the inclination angle of the disk and kT_{in} is the maximum effective temperature in the disk. For the Comptonized component the XSPEC model COMPTT described above was used. The best-fit parameters of the model are shown in Table 5.

The spectral properties of the bright GC X-ray sources detected in the *XMM* observations of the northern disk regions of M31 are similar to that of the bright Galactic low mass X-ray binaries located in the bulge and globular clusters (Sidoli et al. 2001; Iaria et al. 2001; DiSalvo et al. 2001). Two out of total six GC X-ray sources in our sample were found to have X-ray luminosities exceeding 10^{38} ergs s⁻¹, making them brighter than any known Galactic GC X-ray source.

5.2. Variability

The comparisons based on the broad-band spectral properties are not sufficient to establish a neutron star nature or rule out a black hole nature for the M31 globular cluster sources. On the other hand, the study of their short-term variability can provide a definitive answer, if Type I X-ray bursts or X-ray pulsations are observed. We searched for both types of variability in the M31 GC data. Unfortunately, the observed source count rates for most sources are too low to probe timescales shorter than $\sim 20 - 30$ seconds. We did not find evidence of X-ray pulsations or short X-ray bursts in *XMM-Newton* data.

5.3. Correlation between X-ray and optical properties

We used the results of optical observations of M31 GC candidates (Huchra, Brodie & Kent 1991; Barmby et al. 2000; Perrett et al. 2002) to study how the properties of the X-ray sources depend on the overall properties of the globular clusters hosting them.

The Galactic globular clusters hosting bright LMXBs were found to be both denser and more metal-rich (Sidoli et al. 2001). We studied the effect of globular cluster metallicity on the luminosity of the M31 GC sources from our sample. The resulting dependence is shown in Fig. 7 (*left panel*). The tendency of the brightest sources to reside in the more metal poor clusters ($[\text{Fe}/\text{H}] < -1.5$) is obvious. This behavior seems to be in general disagreement with possible correlation between the metallicity and X-ray luminosity found for the bright Galactic GC sources (Sidoli et al. 2001). The limited statistics of our sample (5 M31 GC X-ray sources) does not allow us to draw conclusions on the applicability of our results to the whole M31 globular cluster X-ray source population.

6. SUPERNOVA REMNANTS

There are three SNR candidates in the lists by Braun & Walterbos (1993) and Magnier et al. (1995) coincident with bright XMM sources (sources ## 3, 17 and 21 in Table 2). All three sources were previously detected with *ROSAT*/PSPC and HRI and identified as SNR (Supper et al. 1997, 2001; Magnier et al. 1997).

The energy spectra of these 3 SNR candidates are shown in Fig. 8. We fitted the spectra of SNR candidates with various single component spectral models including a simple power law, thermal bremsstrahlung, black body, Raymond-Smith thermal plasma (RS) (Raymond & Smith 1977), and non-equilibrium ionization collisional plasma (NEI) models with interstellar absorption. The results of the analytical approximation of the *XMM*/EPIC-pn data for SNR candidates are shown in Table 6.

RS and NEI models are often used to study X-ray emission from supernova remnants. These models give the best approximation to the data for two SNR candidate sources ## 3 and 21, which show clear presence of the emission lines in their spectra (Fig. 8; Table 6).

XMMU J004339.1+412654 (#3) Except for the RS and NEI models, other simple spectral models do not provide acceptable fits to the data ($\chi^2/\nu > 2$). For the RS and NEI models, we first fixed the abundances at solar value (Anders & Grevesse 1989). This set of parameters, however, left bump-like residuals indicating that we had overestimated the contribution from O-K, Ne-K and Fe-L shell emission lines. Then we fixed the abundances based on the values determined from optical spectroscopy of the optical counterpart to XMMU J004339.1+412654 (BW57 in Table 2) (Blair et al. 1982): $[\text{N}/\text{H}] = 1.1 \times 10^{-4}$, $[\text{O}/\text{H}] = 3.7 \times 10^{-4}$, $[\text{S}/\text{H}] = 9.3 \times 10^{-6}$ and $[\text{Ne}/\text{H}] = 1.2 \times 10^{-4}$, corresponding to 0.98, 0.44, 0.57 and 1.00 solar abundance. The Fe abundance was fixed at solar value. Finally, for the RS model we allowed the O, Ne and Fe abundances to be free parameters. The fit improved slightly. The best-fit values of the parameters for the approximation of XMMU J004339.1+412654 spectrum with the RS and NEI models are listed in Table 6. Depending on the type of model and a set of model pa-

rameters (Table 6), the estimated corresponding absorbed luminosity of XMMU J004339.1+412654 in the 0.3 – 3.0 keV energy band lies in the range of $(1.8 - 2.0) \times 10^{36}$ ergs s^{-1} .

XMMU J004451.1+412907 (#17) Due to the limited statistics, both RS and simple power law models provide satisfactory approximation to the spectrum of the fainter SNR candidate source XMMU J004451.1+412907 (Fig. 8). Although the EPIC-pn spectrum of XMMU J004451.1+412907 can be fitted well with RS model with free elemental abundances, we were unable to obtain meaningful constraints on the abundances. Therefore, we assume element abundances to be proportional to the solar values, reducing the number of free abundance parameters to one. The best-fit spectral parameters for the approximation of the spectrum of XMMU J004451.1+412907 with RS model are listed in Table 6. The corresponding X-ray luminosity in the 0.3 – 3.0 keV energy band is $\sim 8 \times 10^{35}$ ergs s^{-1} . The absorbed power law model with photon index of $3.4_{-0.4}^{+0.7}$, an equivalent hydrogen column of $1.6_{-0.4}^{+1.0} \times 10^{21}$ cm^{-2} and 0.3 – 3.0 keV flux of 1.3×10^{-14} ergs $s^{-1} cm^{-2}$ also gives satisfactory approximation to the data ($\chi^2/\nu = 0.6$) (Fig. 8).

XMMU J004513.9+413614 (#21) We used RS model with interstellar absorption to approximate the spectrum of SNR candidate XMMU J004513.9+413614. We first fixed the element abundances at solar value (Anders & Grevesse 1989). Then we fixed the abundances based on the values determined from optical spectroscopy of the optical counterpart to XMMU J004339.1+412655 (BW39 in Table 2) (Blair et al. 1982): $[N/H]=6.8 \times 10^{-5}$, $[O/H]=4.5 \times 10^{-4}$, $[S/H]=6.8 \times 10^{-6}$ and $[Ne/H]=1.2 \times 10^{-4}$, corresponding to 0.61, 0.53, 0.42 and 1.00 solar abundance, with the Fe abundance fixed at the solar value. Finally, we allowed the Fe abundance to vary freely. This fit, optimized with Fe at 0.18 solar, was by far the best (Fig. 8, *panel c*). The fit parameters are listed in Table 6. The estimated 0.3 – 3.0 keV X-ray luminosity of XMMU J004513.9+413614 lies in the range of $(0.8 - 1.1) \times 10^{36}$ ergs s^{-1} .

7. FOREGROUND STARS

We found 5 bright *XMM* sources to coincide with objects in the Magnier et al. (1992) and 2MASS catalogs of stars (Table 2) with X-ray spectral properties consistent with that of Galactic foreground stars (Supper et al. 1997; Haberl et al. 2003). All these sources have soft X-ray spectra without significant emission above 2.5 keV and occupy a distinctive area on the X-ray color-color diagram (Fig. 12). The energy spectra of bright sources identified with Galactic foreground stars are shown in Figure 9. To approximate their energy spectra, we used the model of the emission from the optically thin thermal plasma (XSPEC Raymond-Smith model, RS) with characteristic temperature between 0.6 and 0.8 keV and relatively low iron abundance of 0.1 – 0.6 solar, corrected for the low energy absorption (Table 7). For all objects the absorbing column is well below the Galactic value in the direction of M31 (Table 7), further supporting identification as foreground stars. The X-ray spectra and optical properties of 3 of these sources suggest emission from late-type stars with active coronae, also consistent with colors of their

optical counterparts.

Two sources, XMMU J004347.1+412745 (#6) and XMMU J004540.5+420806 (#22) demonstrate significant variability during 2002 Jan. 5 and Jun. 29 *XMM* observations. The X-ray lightcurves of these sources in the 0.2 – 3.0 keV energy range are shown in Fig. 10.

The source XMMU J004347.1+412745 shows a dramatic change of the X-ray flux during 2002, Jan. 5 observation (obs. #1). The source flux history can be described as a combination of a relatively smooth decline (source flux drops ~ 15 times in the first 23 ks of observation) and a number of irregular flares (Fig. 10).

The source XMMU J004540.5+420806 shows significant variability of X-ray flux during 2002, Jun. 29 *XMM* observation (obs. #3). The source brightness changes with a peak flux level ~ 4 times higher than the low flux level (Fig. 10). It should be noted, that during the 2002, Jan. 26 *XMM* observation (obs. #2) the X-ray flux of XMMU J004540.5+420806 appears to be remarkably stable.

8. RADIO SOURCES

The positions of the two bright *XMM* sources not identified as SNR candidates (##16, 28 in Table 2) coincide with bright radio sources detected with VLA all-sky (Condon et al. 1998) and earlier surveys. These two objects are most likely radio galaxies in the background of M31. Both sources have X-ray spectra presented by absorbed power laws with indices between 1.8 and 2.2, typical for this source class (Fig. 11; Table 8).

9. CLUSTER OF GALAXIES XMMU J004624.8+420420

One of the sources detected in the Obs. ##2 and 3, XMMU J004624.8+420420 (#26 in Table 2) was classified as distant cluster of galaxies based on its spatial extent and X-ray spectrum (Kotov, Trudolyubov & Vestrand 2003). X-ray emission of the cluster is clearly detectable up to the radial distance of 3' from its center. X-ray emission from the source was detected previously by ROSAT, and cataloged as RX J0046.4+4204 (Supper et al. 2001), although it was not recognized as an extended object and a galaxy cluster. A joint spectral fit to the data of EPIC-MOS2 and pn cameras with the Raymond-Smith thermal model gives a temperature of a hot gas inside the cluster, $kT_{gas} = 4.3 \pm 0.3$ keV. The X-ray spectrum of XMMU J004624.8+420420 shows prominent iron emission line indicating cluster redshift of $z = 0.293$. For a cosmological model with $H_0 = 50$ $km s^{-1} Mpc^{-1}$, $\Omega_M = 0.3$ and $\Omega_\Lambda = 0.7$ we derive a bolometric luminosity of 1.6×10^{45} erg/s (Kotov, Trudolyubov & Vestrand 2003). We examined optical images of the cluster region and found a concentration of highly reddened galaxies coincident with the central part of XMMU J004624.8+420420, further supporting our interpretation. In addition, we found a relatively bright radio source NVSS J004625+420406 (Condon et al. 1998) located only 16'' away from the emission center of XMMU J004624.8+420420, indicating that it might be radio galaxy belonging to the cluster.

10. POSSIBLE AGN AND OTHER UNIDENTIFIED SOURCES

The majority of the remaining 18 X-ray sources detected in our survey consists of AGN in the background of M31 or X-ray binaries belonging to the galaxy. For

some of these sources there is a close stellar-like counterpart (sources #31, 37), indicating possible AGN origin. For the source #33 a background galaxy is likely optical counterpart. The spectra of most of these objects are hard and can be represented by power laws with indices between 1.5 and 2.3 (Table 9). The corresponding values of the interstellar absorption inferred from their spectra are close to or well above expected Galactic value (Table 9). For some of these sources a high value of measured column density combined with very low brightness of the possible optical counterpart could be explained by AGN intrinsic obscuration. More reliable optical identifications of these obscured AGN candidates are needed to confirm or reject their AGN nature.

11. X-RAY COLOR-COLOR DIAGRAMS

In order to facilitate comparison between spectral properties of different source classes detected in our observations of the northern disk of M31, we constructed their X-ray color-color diagram. We calculated the total number of counts for each source using its corrected EPIC-pn spectra in three energy bands: the soft band (0.3 – 1.0 keV), medium band (1.0 – 2.0 keV) and hard band (2.0 – 7.0 keV). Two X-ray colors were defined for each source as: $HR1 = (S - M)/T$ (soft color) and $HR2 = (H - M)/T$ (hard color), where S , M , and H are the counts in soft, medium and hard bands respectively, and T is the total number of source counts in the 0.3 – 7.0 keV energy range.

Figure 12 shows the X-ray color-color diagram for bright X-ray sources detected in the *XMM-Newton*/EPIC-pn observations of the northern disk of M31. There are two distinct concentrations of sources in this diagram. The first group with $HR1 > 0.3$ includes intrinsically soft sources – SNR candidates and foreground stars. The other densely populated group includes harder sources: GCS, radio sources and unidentified sources (presumably background AGN and X-ray binaries in M31). The X-ray pulsar candidate (possible HMXB) demonstrates harder and much more absorbed spectrum, and lies at an extreme position with $HR1 \sim -0.2$ and $HR2 \sim 0.4$.

Fig. 12 demonstrates that in most cases it is difficult to establish source type using X-ray color alone. Although it helps to outline the difference between sources with soft and hard spectra (like thermal supernova remnants and stars vs. typical high-mass X-ray binaries or black hole candidates in a hard state), it shows no difference between other physically different classes like, for example, X-ray binaries and Crab-like supernova remnants. The combination of low-energy absorption and limited instrument bandpass have significant effect on the source position on the color-color diagram (Di Stefano & Kong 2002; Prestwich et al. 2003). For example, the source with intrinsically super-soft spectrum, if highly absorbed, can easily “migrate” to the region on the color diagram normally occupied by sources with much harder spectra (Di Stefano & Kong 2002). Therefore, additional information, such as X-ray variability, luminosity and source counterparts at other wavelengths, is needed to classify the X-ray source.

12. DIFFUSE X-RAY EMISSION FROM THE DISK OF M31

Previous X-ray studies of M31 were mostly concentrated on the central region of the galaxy. They revealed the pres-

ence of the unresolved soft X-ray emission component in the bulge of M31 distinct from the emission of point-like sources (Primini et al. 1993; Shirey et al. 2001). The situation with the outer disk of M31 is less clear. Previous observations were not sensitive enough or lacked spatial resolution to fully address a question of the existence of the diffuse X-ray component in the disk. Using the data of *Einstein* observations, Trinchieri & Fabbiano (1991) found no requirement for a diffuse component after exclusion of the detected point-like sources. Based on the later observations with *ROSAT*/PSPC, West, Barber & Folgheraiter (1997) report on a detection of a residual unresolved X-ray emission from the outer disk of M31. They conclude that the bulk of this emission could be attributed to the normal stars in the disk of M31.

The observation of M31 North 1 field revealed the presence of soft unresolved soft X-ray emission from the disk of M31. The unresolved emission follows the pattern of the spiral structure and can be traced up to the distance of $\sim 0.5^\circ$ (~ 7 kpc at 760 kpc) from the center of the galaxy (Fig. 13). The unresolved emission includes a large region along the major axis of M31 and a number of smaller regions in the spiral arms. The unresolved emission covers the “inner star-forming ring” of M31 (Haas et al. 1998) and has several local enhancements that are clearly associated with regions of recent star formation (Schmidtobreck, Haas & Lemke 2000).

To characterize the diffuse emission from the disk of M31, we extracted the EPIC-pn spectrum from ~ 65 arcmin² region in the disk at the projected distance of ~ 5 kpc from the center, using the background region outside the disk and eliminating point-like sources from both the source and background regions. To reduce contamination from faint SNR, regions containing undetected optical SNR candidates (Braun & Walterbos 1993; Magnier et al. 1995) were also excluded from source and background extraction regions. The resulting normalized count spectrum is shown in Fig. 14. The spectrum of the unresolved emission is soft and shows possible presence of spectral lines. A crude approximation of its shape in the 0.3 – 2.0 keV energy range with a power law model gives a value of photon index of ~ 4.6 . The spectrum of unresolved emission can be adequately approximated by two-component spectral model including the Raymond-Smith optically thin thermal plasma emission model with a temperature of 0.26 ± 0.05 keV and normalized 0.3 – 2.0 keV flux of $(3 \pm 0.3) \times 10^{-15}$ ergs s⁻¹ cm⁻² arcmin⁻² and a weak power law component with photon index of ~ 1.7 contributing $\lesssim 25\%$ of the total luminosity in the 0.3 – 2.0 keV energy band (Fig. 14).

The spectrum of unresolved emission differs significantly from the cumulative spectrum of faint point-like sources in the same region, which can be presented by absorbed power law model of photon index 1.8 ± 0.1 and absorbing column density $N_H \sim 10^{21}$. The spectral properties of the unresolved emission are somewhat similar to that of the thermal SNR detected in our observations (see Section 6), but both selection procedure and great spatial extent of the unresolved emission make serious spectral contamination from SNR unlikely. This argues strongly that the bulk of the diffuse X-ray emission in the disk of M31 is not simply due to the faint, unresolved X-ray binaries and

SNR. It suggests that there is a significant hot interstellar gas contribution to the diffuse emission, analogous to the hot gas components found in the center of M31 (Shirey et al. 2001), in the disk of M33 (Long et al. 1996; Pietsch et al. 2003), and in our own Galaxy. Another significant contributor to the diffuse emission component could be X-ray emission from normal stars in the disk of M31 (West, Barber, & Folgheraiter 1997).

A weak power law component in the spectrum of unresolved emission still can be due to the combined effect of faint X-ray binaries below our detection limit and some remaining contribution from extracted point-like sources.

13. SUMMARY

A series of deep *XMM-Newton* observations of northern disk of M31 allow a detailed study of spectral and temporal properties of detected X-ray sources down to flux levels of $\lesssim 10^{-13}$ ergs s^{-1} cm^{-2} . The unprecedented sensitivity of EPIC cameras allowed us to detect and study the unresolved soft X-ray emission associated with disk of M31.

We present the results of X-ray analysis of thirty seven of the brightest sources detected in the M31 northern disk fields. Combining the results of X-ray analysis with available data at other wavelengths, we were able to classify $\sim 50\%$, or 19 out of 37 sources.

Two sources in our sample were previously unknown: the hard X-ray source XMMU J004415.8+413057 and a transient supersoft source XMMU J004414.1+412206. A detailed analysis of the timing properties of XMMU J004415.8+413057 revealed possible X-ray pulsations with a period of 197 s. The combination of the unique spectral and timing properties of XMMU J004415.8+413057 would make it the first accreting X-ray pulsar and HMXB candidate detected in M31.

Six X-ray sources were identified with M31 globular clusters (GC). The spectral properties of GC sources were found to be strikingly similar to that of the bright Galactic low mass X-ray binaries located in the bulge and globular clusters (Sidoli et al. 2001; Iaria et al. 2001; DiSalvo et al. 2001). Two GC X-ray sources (XMMU J004251.9+413107 and XMMU J004627.0+420151) have estimated persistent isotropic luminosities above 10^{38} ergs s^{-1} , making them brighter than any known Galactic GC X-ray source. The comparison of the X-ray properties of GC sources with op-

tical properties of their host globular clusters has shown that brighter sources tend to reside in more metal poor clusters (Fig 7, *left panel*).

Three X-ray sources were identified with SNR based on their X-ray spectra and positional coincidence with SNR candidates from optical and radio surveys. We found five bright X-ray sources to coincide with Galactic foreground stars. Two of them demonstrate a remarkable variability of X-ray flux on a time scale of individual *XMM-Newton* observations. Two X-ray sources coincide with radio sources and are probably distant radio galaxies/AGN.

The properties of the remaining 18 bright X-ray sources detected in our survey are consistent with AGN in the background of M31 and X-ray binaries belonging to M31. Many of them show high values of low-energy absorption, which combined with extreme faintness of their possible optical counterparts makes them good candidates for an obscured AGN.

The *XMM-Newton* observations of M31 North 1 field revealed the presence of soft unresolved X-ray emission from the disk of M31. It follows the pattern of the spiral arms and can be traced up to the distance of $\sim 0.5^\circ$ (~ 7 kpc at 760 kpc) from the center of the galaxy. The spectral properties and spatial distribution of the unresolved emission suggest that there is a significant hot interstellar gas contribution to the diffuse emission, analogous to the hot gas components found in the center of M31, in the disks of other external galaxies and in our own Galaxy.

14. ACKNOWLEDGMENTS

Part of this work was done during a summer workshop at the Aspen Center for Physics, S. T. and W. P. are grateful to the Center for their hospitality. Support for this work was provided through NASA Grant NAG5-12390. *XMM-Newton* is an ESA Science Mission with instruments and contributions directly funded by ESA Member states and the USA (NASA). This research has made use of data obtained through the High Energy Astrophysics Science Archive Research Center Online Service, provided by the NASA/Goddard Space Flight Center. This publication makes use of data products from the Two Micron All Sky Survey, which is a joint project of the University of Massachusetts and the Infrared Processing and Analysis Center/California Institute of Technology, funded by NASA and NSF.

REFERENCES

- Anders, E., & Grevesse, N. 1989, *Geochim. Cosmochim. Acta*, 53, 197
- Arnaud, K. 1996, in *Astronomical Data Analysis Software and Systems V*, ASP Conference Series 101, ed. G. Jacoby & J. Barnes (San Francisco: ASP) 17
- Barmby, P., Huchra, J.P., Brodie, J.P., Forbes, D.A., Schroder, L.L., & Grillmar, C.J. 2000, *AJ*, 119, 727
- Barmby, P., & Huchra, J.P. 2001, *ApJ*, 122, 2458
- Battistini, P., et al., 1987, *A&AS*, 67, 447
- Blair, W. P., Kirshner, R. P., & Chevalier, R. A. 1981, *ApJ*, 247, 879
- Blair, W. P., Kirshner, R. P., & Chevalier, R. A. 1982, *ApJ*, 254, 50
- Condon, J.J., Cotton, W.D., Greisen, E.W., Yin, Q.F., Perley, R.A., Taylor, G.B., & Broderick J.J. 1998, *AJ*, 115, 1693
- DiSalvo, T., Robba, N. R., Iaria, R., Stella, L., Burderi, L., & Israel, G. L. 2001, *ApJ*, 554, 49
- Di Stefano, R., Kong, A. K. H., Garcia, M. R., Barmby, P., Greiner, J., Murray, S. S., & Primini, F. A. 2002, *ApJ*, 570, 618
- Di Stefano, R., & Kong, A. K. H. 2002, *ApJ*, 592, 884
- Dickey, J. M., & Lockman F. J. 1990, *ARA&A*, 28, 215
- Dove, J. B., Wilms, J., Maisack, M., & Begelman, M. C. 1997, *ApJ*, 487, 759
- Garcia, M. R., Kong, A. K. H., McClintock, J. E., Primini, F. A., Kaaret, P., & Murray, S. S. 2002, *Atel*, 82
- Haas, M., Lemke, D., Stickel, M., Hippelein, H., Kunkel, M., Herbstmeier, U., & Mattila, K. 1998, *A&A*, 338, L33
- Haberl, F., Dennerl, K., & Pietsch, W. 2003, *A&A*, 406, 471
- Haiman, Z., Magnier, E. A., Lester, R. R., Lewin, W. H. G., van Paradijs, J., Hasinger, G., Pietsch, W., & Truemper, J. 1994, *A&A*, 286, 725
- Huchra, J.P., Brodie, J.P., & Kent, S.M. 1991, *ApJ*, 370, 495
- Iaria, R., Burderi, L., Di Salvo, T., La Barbera, A., & Robba, N. R. 2001, *ApJ*, 547, 412
- Kahabka, P., & van den Heuvel, E. P. J. 1997, *ARA&A*, 35, 69
- Kong, A. K. H., Garcia, M. R., Primini, F. A., Murray, S. S., Di Stefano, R., & McClintock, J. E. 2002, *ApJ*, 577, 738
- Kotov, O., Rudolyubov, S., & Vestrand, W. T. 2003, *ApJ*, submitted
- Long, K., Charles, P., Blair, W., & Gordon, S. 1996, *ApJ*, 466, 750
- Magnier, E. A., Lewin, W. H. G., van Paradijs, J., Hasinger, G., Jain, A., Pietsch, W., & Truemper, J. 1992, *A&AS*, 96, 379

- Magnier, E. A. 1993, Ph.D. thesis, MIT
Magnier, E. A., Prins, S., van Paradijs, J., Lewin, W. H. G., Supper, R., Hasinger, G., Pietsch, W., Truemper, J. 1995, A&AS, 114, 215
Magnier, E. A., Primini, F. A., Prins, S., van Paradijs, J., & Lewin, W. H. G. 1997, ApJ, 490, 649
Massey, P., Hodge, P. W., Holmes, S., Jacoby, G., King, N. L., Olsen, K., Saha, A., & Smith, C. 2001, in American Astronomical Society Meeting, 199, 1305
Mitsuda, K., Inoue, H., Koyama, K., et al. 1984, PASJ, 36, 741
Perrett, K.M., Bridges, T.J., Hanes, D.A., Irwin, M.J., Brodie, J.P., Carter, D., Huchra, J.P., & Watson, F.G. 2002, AJ, 123, 2490
Pietsch, W., Ehle, M., Haberl, F., Misanovic, Z., Trinchieri, G. 2003, Astronomische Nachrichten, 324, 85
Prestwich, A. H., Irwin, J. A., Kilgard, R. E., Krauss, M. I., Zezas, A., Primini, F., Kaaret, P., & Boroson, B. 2003, ApJ, 595, 719
Primini, F. A., Forman, W., & Jones, C., 1993, ApJ, 410, 615
Ramsay, G., Mason, K. O., Cropper, M., Watson, M. G., & Clayton, K. L. 1994, MNRAS, 270, 692
Raymond, J. S., & Smith, B. W. 1977, ApJS, 35, 419
Schmidtobreick, L., Haas, M., & Lemke, D. 2000, A&A, 363, 917
Shirey, R., Soria, R., Borozdin, K., Osborne, J. P., Tiengo, A., Guainazzi, M., Hayter, C., La Palombara, N., Mason, K., Molendi, S., Paerels, F., Pietsch, W., Priedhorsky, W., Read, A. M., Watson, M. G., West, R. G., 2001, A&A, 365, L195
Sidoli, L., Parmar, A. N., Oosterbroek, T., Stella, L., Verbunt, F., Masetti, N., & Dal Fiume, D., 2001, A&A, 368, 451
Strueder, L. et al., 2001, A&A, L18
Sunyaev, R. A., & Titarchuk, L. G. 1980, A&A, 86, 121
Supper, R., Hasinger, G., Pietsch, W., Truemper, J., Jain, A., Magnier, E.A., Lewin, W.H.G., & van Paradijs, J. 1997, A&A, 317, 328
Supper, R., Hasinger, G., Lewin, W. H. G., Magnier, E.A., van Paradijs, J., Pietsch, W., Read, A.M., & Truemper, J. 2001, A&A, 373, 63
Titarchuk, L. 1994, ApJ, 434, 570
Titarchuk, L., & Lyubarskij, Y. 1995, ApJ, 450, 876
Trinchieri, G., & Fabbiano, G., 1991, ApJ, 382, 82
Trudolyubov, S., Borozdin, K., & Priedhorsky, W., Mason, K., & Cordova, F. 2002, IAU Circ. 7798
Trudolyubov, S., Borozdin, K., & Priedhorsky, W., Osborne, J., Watson, M., Mason, K., & Cordova, F. 2002b, ApJ, 581, L27
Turner, M. et al., 2001, A&A, 365, L27
Vaughan, B. A., van der Klis, M., Wood, K. S., Norris, J. P., Hertz, P., Michelson, P. F., van Paradijs, J., Lewin, W. H. G., Mitsuda, K., & Penninx, W. 1994, ApJ, 435, 362
West, R. G., Barber, C. R., & Folgheraiter, E. L. 1997, MNRAS, 287, 10
Williams, B. F., Garcia, M. R., Kong, A. K. H., Primini, F. A., King, A. R., & Murray, S. S. 2003, ApJ, submitted, astro-ph/0306421

TABLE 1
XMM-NEWTON OBSERVATIONS OF M31 NORTH1, NORTH2 AND NORTH3 FIELDS.

Obs. #	Date, UT	T_{start} , UT (h:m:s)	Field	Obs. ID	RA (J2000) ^a (h:m:s)	Dec (J2000) ^a (d:m:s)	Exp.(MOS) ^b (ks)	Exp.(pn) ^b (ks)
#1	2002 Jan 05	06:28:31	M31 North1	0109270701	00:44:01.0	41:35:57.0	57.3	54.7
#2	2002 Jan 26	16:51:03	M31 North2	0109270301	00:45:20.0	41:56:09.0	29.1	25.3
#3	2002 Jun 29	08:59:02	M31 North3	0109270401	00:46:38.0	42:16:20.0	51.5	36.5
#4	2002 Jan 06	18:07:17	M31 Core	0112570101	00:42:43.0	41:15:46.1	63.0	61.0

^a – coordinates of the center of the field of view

^b – instrument exposure used in the analysis

TABLE 2
 SAMPLE OF SELECTED BRIGHT X-RAY SOURCES IN THE EPIC OBSERVATIONS OF NORTHERN DISK FIELDS OF M31

Source ID	<i>XMM</i> Source Name (XMMU ...)	Optical/IR/Radio ID ^a	Offset ^b (")	SHP97 ^c	Offset ^d (")	Comment
1	J004251.9+413107	Bo 135	1.4	205	1.8	GCS
2	J004301.3+413017	Bo 91/MIT 236	0.9	218	5.3	GCS
3	J004339.1+412654	BW57/MA 3-069	2.3/6.9	249	5.6	SNR
		W85 180	2.2			
4	J004342.9+412850	MIT 311	1.3	250	1.4	GCS
		MLV92 315558	1.0			
5	J004345.5+413657	Bo 193	1.2	253	4.4	GCS
6	J004347.1+412745	2MASS 004347.18+412744.5	1.6			Foreground star
		MLV92 308951	1.8			
7	J004356.5+412202	Bo204	0.6	261	3.5	GCS
8	J004357.5+413054	MLV92 328135	1.3	268	2.1	
9	J004402.7+413927	MLV92 379667	1.0	266	4.1	
10	J004412.0+413147	MLV92 333307	0.9	272	4.7	
11	J004414.1+412206					Supersoft transient
12	J004415.8+413057					Transient, HMXB? 197s pulsar
13	J004422.5+414507	MLV92 394966	0.3	278	3.3	
14	J004424.7+413200	MLV92 334722	0.7	279	12	
		MLV92 334827	1.7			
15	J004425.5+413633	2MASS 004425.57+413633.4	0.6	281	6.0	Foreground star
		MLV92 362312	0.4			
16	J004437.8+414513	NVSS J004437+414511	2.0			Radio source
		W85 207	6.5			
17	J004451.1+412907	BW 33	2.6	288	16	SNR
18	J004452.2+412717	MLV92 306564	2.2	289	2.4	
		MLV92 306271	2.5			
19	J004455.4+413440					
20	J004456.3+415936	2MASS 004456.37+415936.8	0.4	292	7.0	Foreground star
		MLV92 436498	0.6			
21	J004513.9+413614	BW 39/MA 2-049	1.7/4.1	297	9.1	SNR
		W85 231	4.7			
22	J004540.5+420806	2MASS 004540.54+420806.8	0.8	316	4.0	Foreground star
		MLV92 450979	0.6			
23	J004544.9+415858			317	2.6	
24	J004611.5+420826			332	5.3	
25	J004619.9+421441	MLV92 462752	1.6			
		MLV92 462656	4.3			
26	J004624.8+420420	NVSS J004625+420406	16	348	19	Cluster of Galaxies at $z = 0.3$
27	J004627.0+420151	Bo 386	1.2	349	4.0	GCS
28	J004648.0+420851	NVSS J004648+420855	3.8	353	1.8	Radio source
		W85 252	2.8			
29	J004651.8+421951			354	12	
30	J004651.9+421504					
31	J004655.4+422049	2MASS 004655.51+422050.1	1.6	355	4.1	
		MLV92 472612	1.4			
32	J004703.6+420449	MLV92 444881	3.7	357	5.6	
33	J004706.5+422211	MLV92 474281	1.9	359	12	
34	J004713.3+422045	MLV92 472554	2.2	361	11	
35	J004725.2+422118	MLV92 473224	2.0			
36	J004726.1+422157	2MASS 004726.12+422158.4	1.6	369	6.1	Foreground star
		MLV92 474007	1.4			
37	J004748.3+421932	MLV92 470983	1.8	384	7.1	

^a – source identifications beginning with BW refer to the SNR candidates listed in Braun & Walterbos (1993). Identifications beginning with MA refer to the SNR candidates from Magnier et al. (1995). Identifications beginning with Bo refer to M31 Globular Cluster candidates listed in Table IV of Battistini et al. (1987). Identifications beginning with MIT refer to M31 Globular cluster candidates from Magnier (1993).

^b – angular distance between *XMM* source position and the position of its possible optical counterpart.

^c – SHP97 refer to M31 *ROSAT*/PSPC catalogue entries from Supper et al. (1997, 2001).

^d – offset between *XMM* and *ROSAT* source positions.

TABLE 3
SPECTRAL FIT RESULTS FOR BRIGHT SOURCES DISCOVERED WITH *XMM-Newton*.

Parameter	
XMMU J004415.8+413057 ^a (#12)	
Absorbed Power Law	
Photon Index	1.43 ^{+0.19} _{-0.11}
$N_{\text{H}}, \times 10^{22} \text{ cm}^{-2}$	1.36 ^{+0.47} _{-0.26}
Flux ^b	1.29 ± 0.07
$\chi^2(\text{d.o.f.})$	16.1(20)
XMMU J004414.1+412206 ^c (#11)	
Absorbed Black Body Model	
$kT_{\text{bb}}, \text{eV}$	34 ± 3
$N_{\text{H}}, \times 10^{22} \text{ cm}^{-2}$	0.43 ± 0.03
Flux ^d	1.11 ± 0.04
$\chi^2(\text{dof})$	88.6(33)

^a – EPIC-pn data, 0.3 – 10 keV energy range

^b – Absorbed model flux in the 0.3 – 10.0 keV energy range in units of $10^{-13} \text{ erg s}^{-1} \text{ cm}^{-2}$

^c – EPIC-MOS1 and MOS2 data, 0.2 – 1.0 keV energy range

^d – Absorbed model flux in the 0.3 – 1.0 keV energy range in units of $10^{-13} \text{ erg s}^{-1} \text{ cm}^{-2}$

TABLE 4
BRIGHT GCS SPECTRAL FIT RESULTS (*XMM-Newton*/EPIC DATA, 0.3 – 10 keV ENERGY RANGE).

ID ^a	Model: Absorbed Power Law (POWERLAW*WABS)					Remarks	
	Photon Index	N_{H}^b	Flux ^c	χ^2 (dof)	L_X^d		
01	1.57 ^{+0.03} _{-0.02}	0.26 ± 0.01	52.95 ± 0.42	443.7(424)	3651	MOS1+MOS2	
02	0.83 ± 0.04	0.07 ^{+0.01} _{-0.02}	8.91 ± 0.19	228.6(176)	614	MOS1+MOS2+pn	
04	1.61 ^{+0.14} _{-0.13}	0.23 ± 0.05	0.75 ± 0.05	33.2(32)	52	pn	
05	1.61 ^{+0.13} _{-0.04}	0.04 ± 0.03	0.64 ± 0.03	26.3(26)	44	MOS1+MOS2	
07	1.90 ± 0.32	0.19 ± 0.07	0.54 ± 0.05	14.6(16)	37	pn	
27	1.55 ^{+0.04} _{-0.03}	0.13 ± 0.01	21.66 ± 0.30	270.2(237)	1493	MOS1+MOS2+pn	
Model: Absorbed Cutoff Power Law (CUTOFFPL*WABS)							
	Photon Index	Cutoff Energy (keV)	N_{H}^b	Flux ^c	χ^2 (dof)	L_X^d	
01	0.84 ± 0.11	4.20 ^{+0.76} _{-0.57}	0.16 ^{+0.02} _{-0.01}	47.80 ± 0.40	399.3(423)	3296	
02	0.18 ± 0.09	4.86 ^{+1.12} _{-0.72}	< 0.02	7.91 ± 0.17	208.0(175)	545	
27	1.16 ^{+0.16} _{-0.17}	7.49 ^{+5.33} _{-2.17}	0.09 ^{+0.01} _{-0.02}	20.44 ± 0.29	264.4(236)	1409	
Model: Absorbed Comptonization Model (COMPTT*WABS)							
	kT_0 (keV)	kT_e (keV)	Optical Depth	N_{H}^b	Flux ^c	χ^2 (dof)	L_X^d
01	0.37 ^{+0.01} _{-0.03}	1.88 ^{+0.23} _{-0.18}	19.5 ^{+0.9} _{-1.6}	< 0.02	47.82 ± 0.41	398.7(422)	3297
02	0.03 ^{+0.07} _{-0.01}	1.76 ^{+0.14} _{-0.12}	34.6 ^{+2.8} _{-2.5}	0.07 ^{+0.01} _{-0.02}	7.38 ± 0.16	206.8(174)	509
27	0.14 ± 0.04	1.64 ^{+0.15} _{-0.16}	22.4 ^{+2.2} _{-2.3}	0.09 ± 0.02	19.42 ± 0.28	258.3(235)	1339

^a – Source number in Table 2

^b – Equivalent hydrogen column depth in units of 10^{22} cm^{-2}

^c – Absorbed model flux in the 0.3 – 10 keV energy range in units of $10^{-13} \text{ erg s}^{-1} \text{ cm}^{-2}$

^d – Absorbed isotropic source luminosity in the 0.3 – 10.0 keV energy range in units of $10^{35} \text{ erg s}^{-1}$ assuming the distance of 760 kpc

TABLE 5

SPECTRAL FIT RESULTS FOR THE APPROXIMATION OF THE EPIC-MOS SPECTRA OF XMMU J004251.9+413107 WITH COMBINATION OF ABSORBED COMPTONIZATION AND DISK-BLACKBODY MODELS.

Parameter	
XMMU J004251.9+413107 ^a (#1)	
(COMPTT+DISKBB)*WABS	
$N_{\text{H}}, \times 10^{22} \text{ cm}^{-2}$	0.14 ± 0.02
$kT_0, \text{ keV}$	$0.58^{+0.09}_{-0.11}$
$kT_e, \text{ keV}$	$2.14^{+1.56}_{-0.43}$
Optical Depth	$17.4^{+3.6}_{-11.1}$
$kT_{in}, \text{ keV}$	$0.53^{+0.13}_{-0.19}$
$r_{in} \sqrt{\cos i}, \text{ km}$	68^{+96}_{-30}
Flux ^b	48.54 ± 0.41
f_{soft}^c	0.23
$\chi^2(\text{d.o.f.})$	391.9(420)
L_X^d	3347

^a – EPIC-MOS1 and MOS2 data, 0.3 – 10 keV energy range

^b – Absorbed model flux in the 0.3 – 10.0 keV energy range in units of $10^{-13} \text{ erg s}^{-1} \text{ cm}^{-2}$

^c – Absorption-corrected ratio of the disk-blackbody flux to the total source flux in the 0.3 – 10.0 keV energy band

^d – Absorbed isotropic source luminosity in the 0.3 – 10.0 keV energy range in units of $10^{35} \text{ erg s}^{-1}$ assuming the distance of 760 kpc

TABLE 6

BRIGHT SNR CANDIDATE SOURCES SPECTRAL FIT RESULTS (*XMM-Newton*/EPIC DATA, ABSORBED RS AND NEI MODELS, *XMM*/EPIC-PN DATA 0.3 – 3.0 keV ENERGY RANGE.

Model	kT_{RS}/kT_e (keV)	$\log n_e t$	Abundance ^a					N_{H}^b	Flux ^c	$\chi^2/(\text{dof})$
			N	O	Ne	S	Fe			
XMMU J004339.1+412654 (#3)										
RS	$0.09^{+0.01}_{-0.01}$...	1	1	1	1	1	$0.88^{+0.06}_{-0.08}$	0.26 ± 0.02	39.8(34)
	$0.12^{+0.02}_{-0.01}$...	0.98^d	0.44^d	1.00^d	0.57^d	1	$0.61^{+0.08}_{-0.14}$	0.26 ± 0.02	36.5(34)
	$0.26^{+0.03}_{-0.04}$...	0.98^d	0.19 ± 0.07	$0.64^{+0.30}_{-0.24}$	0.57^d	$0.15^{+0.08}_{-0.05}$	$0.11^{+0.09}_{-0.04}$	0.29 ± 0.02	26.3(31)
NEI	$0.22^{+0.07}_{-0.04}$	$10.8^{+0.4}_{-0.2}$	1	1	1	1	1	$0.52^{+0.08}_{-0.03}$	0.26 ± 0.02	46.0(33)
	$1.06^{+0.98}_{-0.53}$	$9.9^{+0.2}_{-0.1}$	0.98^d	0.44^d	1.00^d	0.57^d	1	$0.14^{+0.09}_{-0.08}$	0.29 ± 0.02	33.1(33)
XMMU J004513.9+413614 (#21)										
RS	0.24 ± 0.06	...	1	1	1	1	1	$0.54^{+0.14}_{-0.18}$	0.13 ± 0.01	15.3(14)
	$0.24^{+0.07}_{-0.06}$...	0.61^d	0.53^d	1.00^d	0.42^d	1	$0.47^{+0.13}_{-0.25}$	0.12 ± 0.01	19.4(14)
	$0.45^{+0.10}_{-0.04}$...	0.61^d	0.53^d	1.00^d	0.42^d	$0.18^{+0.09}_{-0.06}$	$0.09^{+0.08}_{-0.06}$	0.16 ± 0.01	9.8(13)
XMMU J004451.1+412907 (#17)										
RS	$0.67^{+0.60}_{-0.18}$...	< 0.01	< 0.01	< 0.01	< 0.01	< 0.01	$0.07^{+0.04}_{-0.06}$	0.12 ± 0.01	7.9(10)

^a – Relative to the solar abundance.

^b – An equivalent hydrogen column density in units of 10^{22} cm^{-2} .

^c – Absorbed model flux in the 0.3 – 3.0 keV energy range in units of $10^{-13} \text{ erg s}^{-1} \text{ cm}^{-2}$.

^d – Fixed at optical value (Blair et al. 1982).

TABLE 7

BRIGHT GALACTIC FOREGROUND STARS ABSORBED RS MODEL SPECTRAL FIT RESULTS (*XMM-Newton*/EPIC DATA, 0.3 – 3.0 KEV ENERGY RANGE).

Source ID	kT (keV)	A_{Fe}	N_{H} $\times 10^{21} \text{ cm}^{-2}$	Flux ^a	χ^2 (dof)	Remarks
6	$0.84^{+0.05}_{-0.07}$	$0.16^{+0.09}_{-0.06}$	0.34^b	0.21 ± 0.02	19.5(19)	pn
15	$0.79^{+0.04}_{-0.06}$	$0.30^{+0.09}_{-0.07}$	0.31^b	0.22 ± 0.01	45.6(24)	pn
20	$0.80^{+0.05}_{-0.08}$	$0.13^{+0.06}_{-0.05}$	0.12^b	0.50 ± 0.02	34.9(22)	pn
22	$0.66^{+0.04}_{-0.03}$	$0.17^{+0.03}_{-0.07}$	0.06^b	1.24 ± 0.06	58.8(29)	pn, Obs. #2
22	0.65 ± 0.02	0.10 ± 0.03	0.02^b	2.70 ± 0.06	149.3(91)	pn+MOS1, Obs. #3
36	$0.66^{+0.03}_{-0.04}$	$0.57^{+0.15}_{-0.11}$	$0.27^{+0.40}_{-0.27}$	0.32 ± 0.02	31.9(33)	pn+MOS1+MOS2

^a – absorbed model flux in the 0.3 – 3.0 keV energy range in units of $10^{-13} \text{ erg s}^{-1} \text{ cm}^{-2}$

^b – a 2σ upper limit

TABLE 8

RADIO SOURCES SPECTRAL FIT RESULTS (*XMM-Newton*/EPIC DATA, ABSORBED SIMPLE POWER LAW MODEL, 0.3 – 10.0 KEV ENERGY RANGE).

Source ID	Photon Index	N_{H} $\times 10^{22} \text{ cm}^{-2}$	Flux ^a	χ^2 (dof)	Remarks
16	$2.15^{+0.11}_{-0.13}$	$0.17^{+0.03}_{-0.04}$	0.73 ± 0.06	19.1(25)	pn
28	$1.86^{+0.10}_{-0.12}$	$0.40^{+0.10}_{-0.05}$	1.00 ± 0.04	61.3(50)	pn+MOS1+MOS2

^a – absorbed model flux in the 0.3 – 10 keV energy range in units of $10^{-13} \text{ erg s}^{-1} \text{ cm}^{-2}$

TABLE 9

OTHER BRIGHT X-RAY SOURCES SPECTRAL FIT RESULTS (*XMM-Newton*/EPIC DATA, ABSORBED SIMPLE POWER LAW MODEL, 0.3 – 10 KEV ENERGY RANGE).

Source Name XMMU J00...	Photon Index	N_{H} $\times 10^{22} \text{ cm}^{-2}$	Flux ^a	χ^2 (dof)	Remarks
8	$1.62^{+0.13}_{-0.09}$	$0.06^{+0.02}_{-0.04}$	0.62 ± 0.03	47.5(44)	pn
9	$2.88^{+0.40}_{-0.30}$	$0.72^{+0.21}_{-0.23}$	0.19 ± 0.02	13.7(17)	pn
10	$1.91^{+0.13}_{-0.15}$	$0.12^{+0.04}_{-0.05}$	0.33 ± 0.02	9.6(20)	pn
13	1.85 ± 0.10	0.06 ± 0.03	1.65 ± 0.07	23.3(35)	MOS1+MOS2
14	1.97 ± 0.07	$0.19^{+0.02}_{-0.03}$	1.16 ± 0.04	60.4(57)	pn+MOS1+MOS2
18	$1.79^{+0.17}_{-0.17}$	$0.10^{+0.04}_{-0.06}$	1.40 ± 0.10	5.9(11)	MOS2
19	$1.55^{+0.21}_{-0.16}$	$0.47^{+0.19}_{-0.11}$	1.72 ± 0.11	31.2(43)	MOS1+MOS2
23	$2.05^{+0.23}_{-0.18}$	$0.30^{+0.08}_{-0.06}$	0.54 ± 0.04	12.6(13)	pn
24	$1.67^{+0.08}_{-0.07}$	$0.25^{+0.03}_{-0.04}$	1.19 ± 0.05	40.1(45)	pn+MOS1+MOS2
25	$1.61^{+0.14}_{-0.13}$	$0.18^{+0.08}_{-0.06}$	0.74 ± 0.04	22.9(28)	MOS1+MOS2
29	$1.78^{+0.30}_{-0.24}$	$0.30^{+0.16}_{-0.09}$	0.34 ± 0.03	10.6(14)	pn
30	1.54 ± 0.29	$0.10^{+0.08}_{-0.05}$	0.27 ± 0.02	13.3(8)	pn
31	$2.29^{+0.05}_{-0.04}$	0.15 ± 0.01	4.75 ± 0.06	319.5(295)	pn+MOS1+MOS2
32	$1.79^{+0.23}_{-0.19}$	0.23 ± 0.06	0.91 ± 0.08	10.1(13)	pn
33	$1.39^{+0.38}_{-0.22}$	$0.16^{+0.21}_{-0.08}$	0.67 ± 0.06	23.8(14)	pn
34	$1.94^{+0.09}_{-0.08}$	0.10 ± 0.03	0.87 ± 0.03	55.1(58)	pn+MOS1+MOS2
35	$1.61^{+0.17}_{-0.18}$	0.10 ± 0.06	0.56 ± 0.05	12.8(15)	pn
37	$1.73^{+0.07}_{-0.08}$	$0.23^{+0.02}_{-0.03}$	5.83 ± 0.14	76.4(71)	MOS1+MOS2

^a – absorbed model flux in the 0.3 – 10 keV energy range in units of $10^{-13} \text{ erg s}^{-1} \text{ cm}^{-2}$

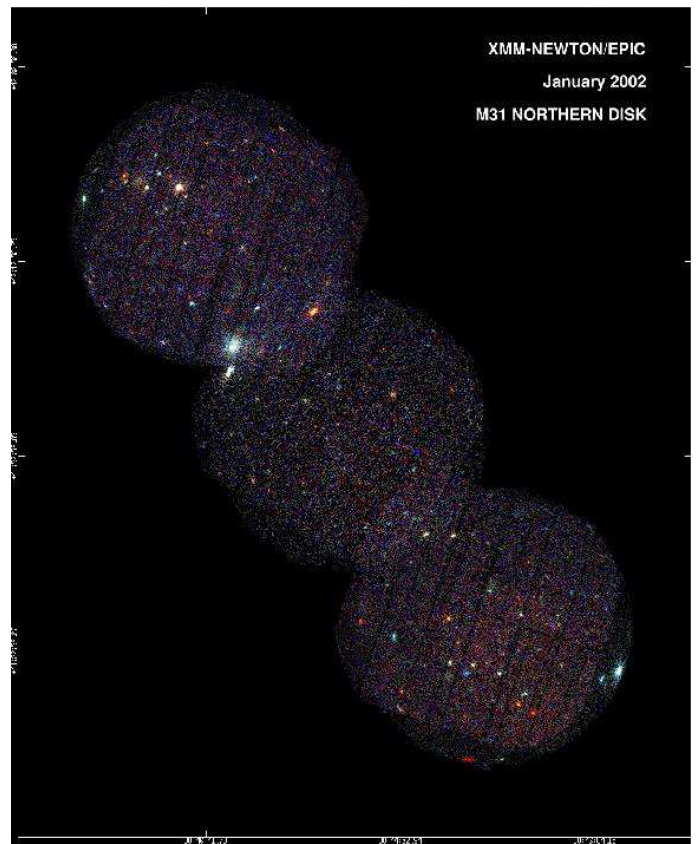
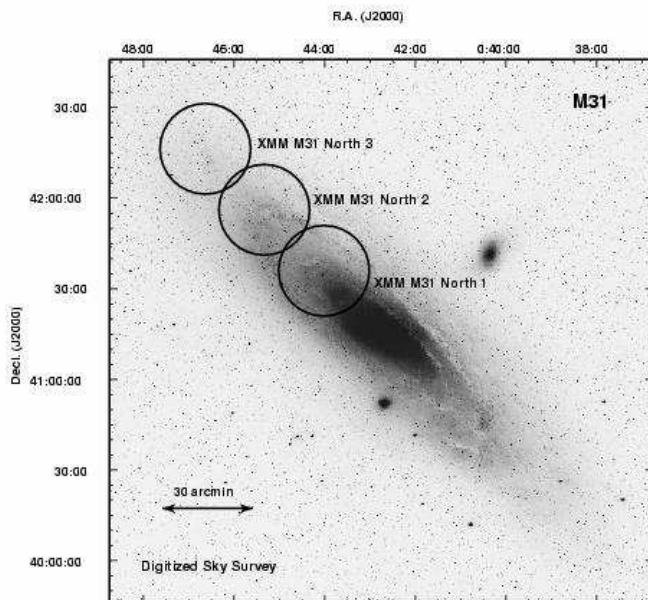


FIG. 1.— *Left*: Optical image of M31 from Digitized Sky Survey with *XMM-Newton* FOV shown as circles for each of the M31 North 1, North 2 and North 3 fields from Table 1. *Right*: A detailed three-color combined *XMM-Newton*/EPIC X-ray image of the northern disk of M31. The red, green and blue intensities correspond to logarithmically scaled counts in the 0.3 – 1.0, 1.0 – 2.0 and 2.0 – 7.0 keV energy bands. The image was constructed with $2''$ pixels.

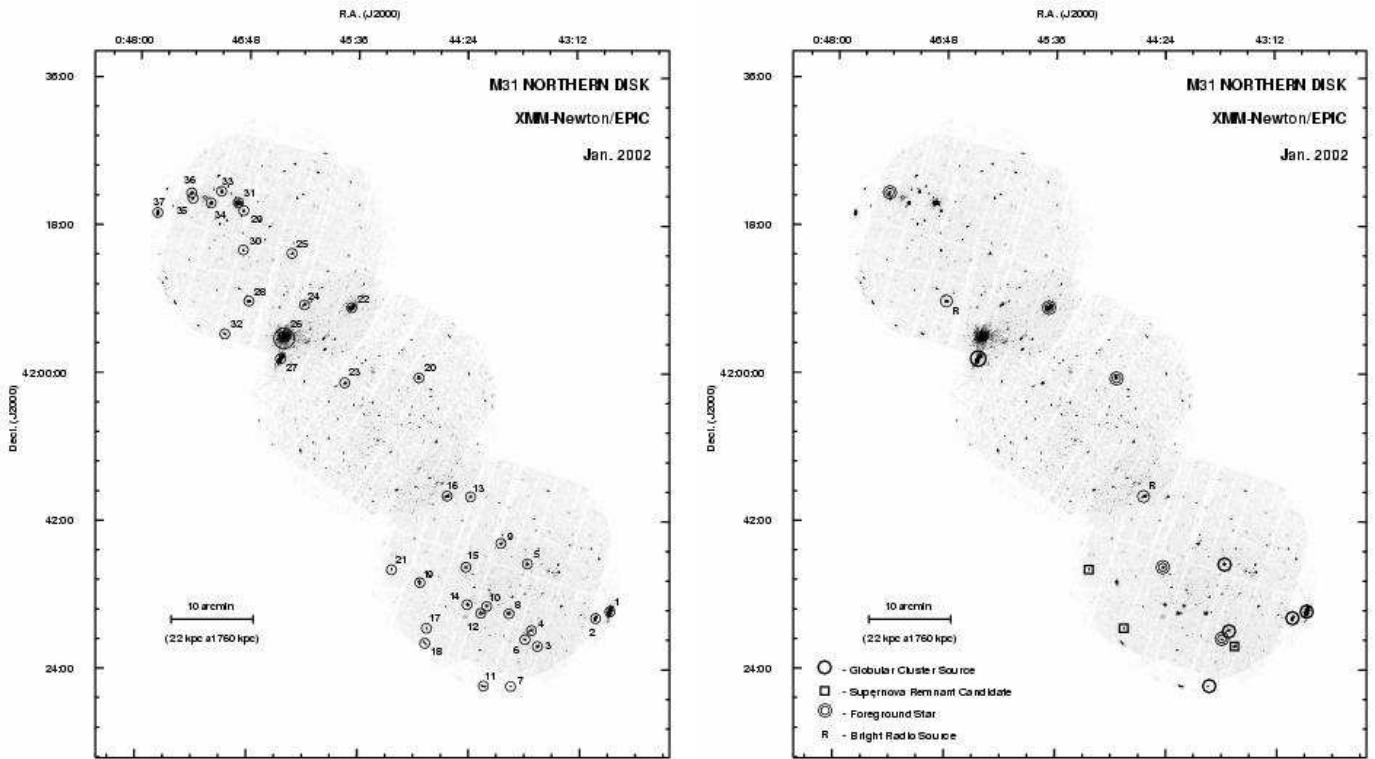


FIG. 2.— *Left:* Combined *XMM-Newton*/EPIC image of the M31 North1, North2 and North3 disk fields (Table 1). Positions of the selected bright X-ray sources detected with *XMM-Newton*/EPIC cameras are marked with small circles. Source labels correspond to the numbering in Table 2. *Right:* Combined *XMM-Newton*/EPIC image of the M31 North1, North2 and North3 disk fields with optical/radio identifications of the selected bright XMM sources from Table 2.

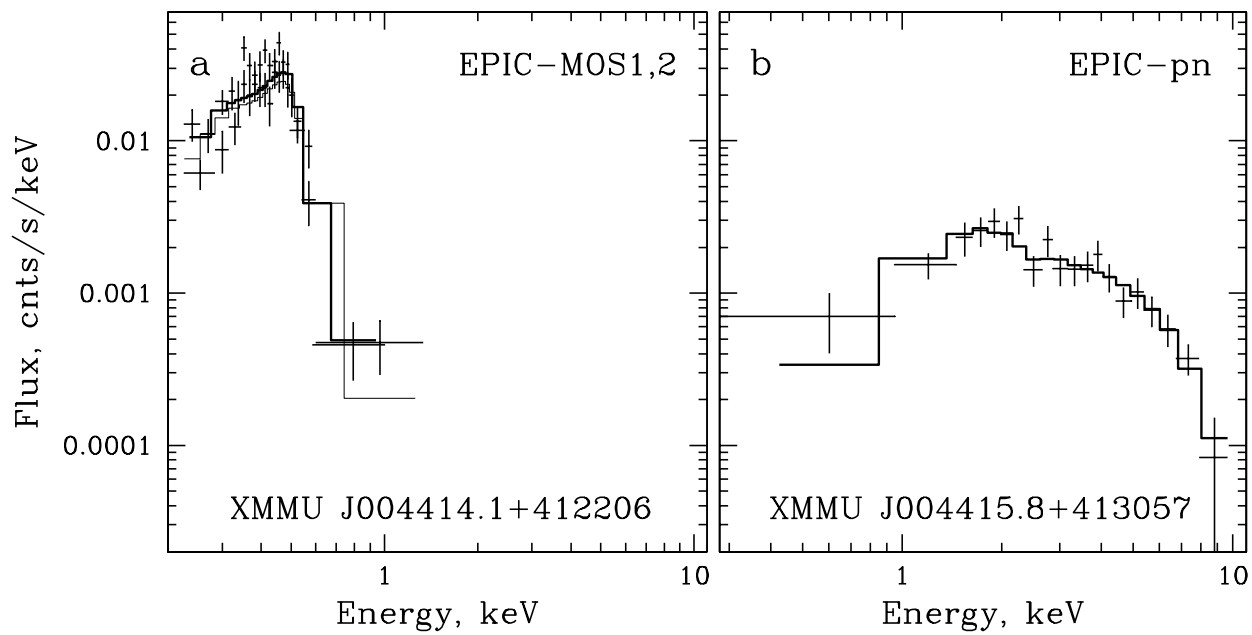


FIG. 3.— Count spectra of bright transient sources. EPIC data, 0.3–10 keV energy range. (a) Transient supersoft source XMMU J004414.1+412206, EPIC-MOS1 and MOS2 data, fit by the absorbed black body radiation model. The fits to EPIC-MOS1 and MOS2 data are shown with *thick* and *thin* histograms. (b) Hard X-ray transient source XMMU J004415.8+413057, EPIC-pn data, fit by the absorbed simple power law model.

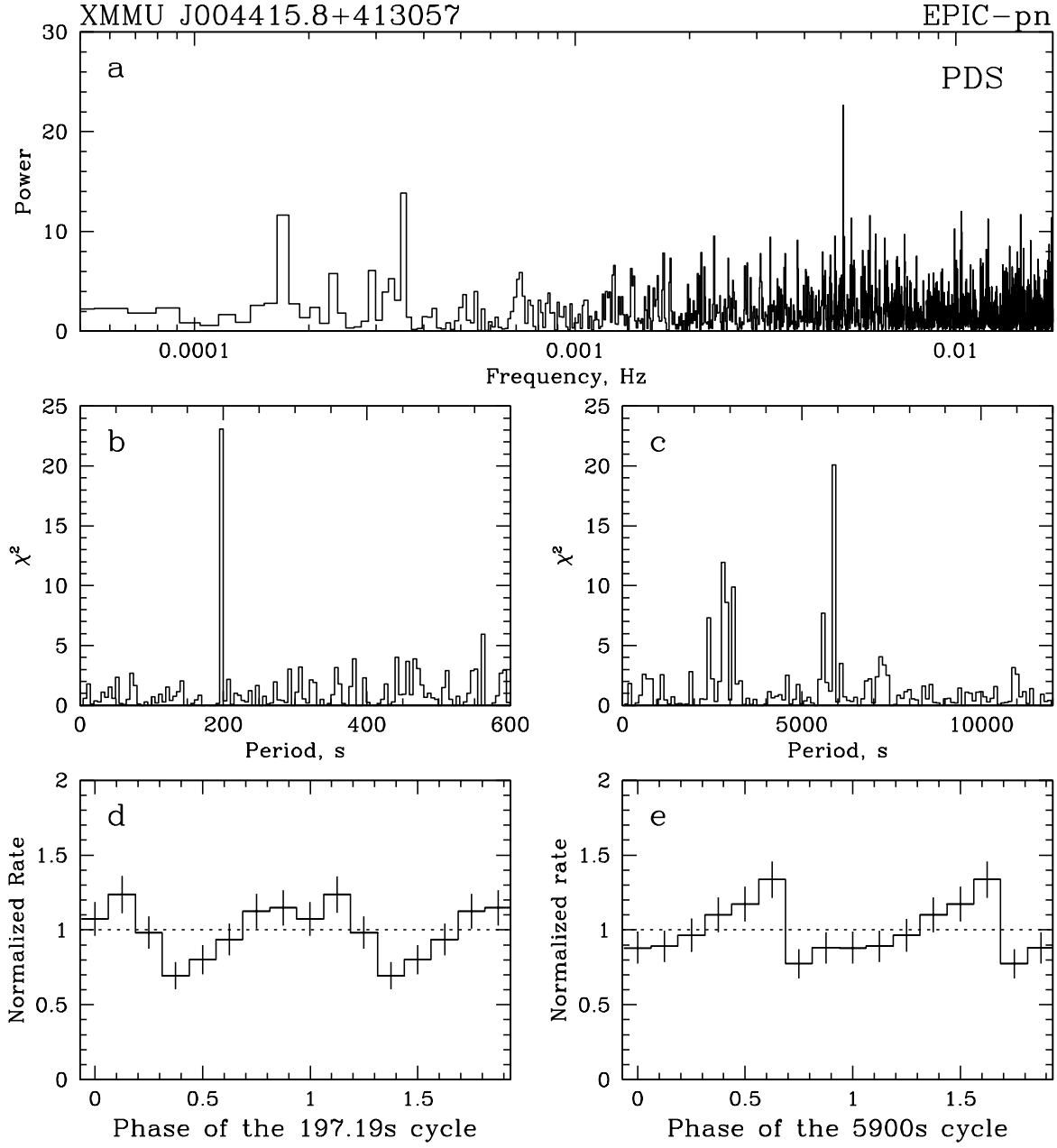


FIG. 4.— The results of timing analysis of the light curve of XMMU J004415.8+413057 (EPIC-pn data, 0.3 – 7.0 keV energy band). (a) Power density spectrum of XMMU J004415.8+413057 showing possible X-ray pulsations with a period of 197 s and a slower 5900 s modulation. (b,c) Resulting χ^2 distributions for the epoch-folding analysis of the X-ray light curve of the source. The best-fit periods of the modulations are 197.19 s and 5900 s respectively. (d,e) Normalized light curves of the source, folded at the best-fit periods of 197.19 s and 5900 s.

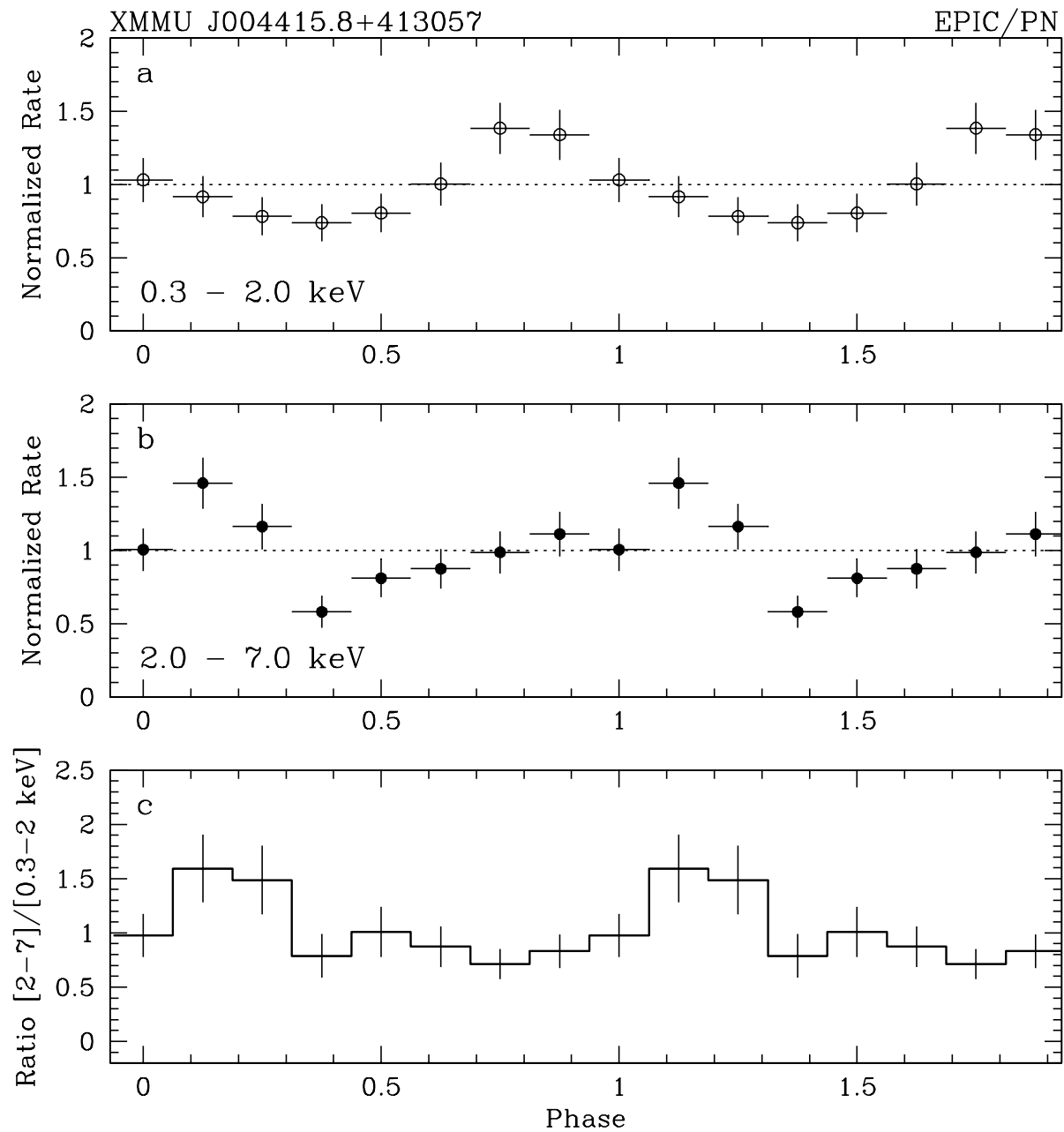


FIG. 5.— (a,b) X-ray light curves of XMMU J004415.8+413057 in the 0.3 – 2.0 and 2.0 – 7.0 keV energy bands taken with EPIC-pn, folded on a period of 197.19 s. (c) Hardness of the source spectrum as a function of phase of 197.19 s modulation.

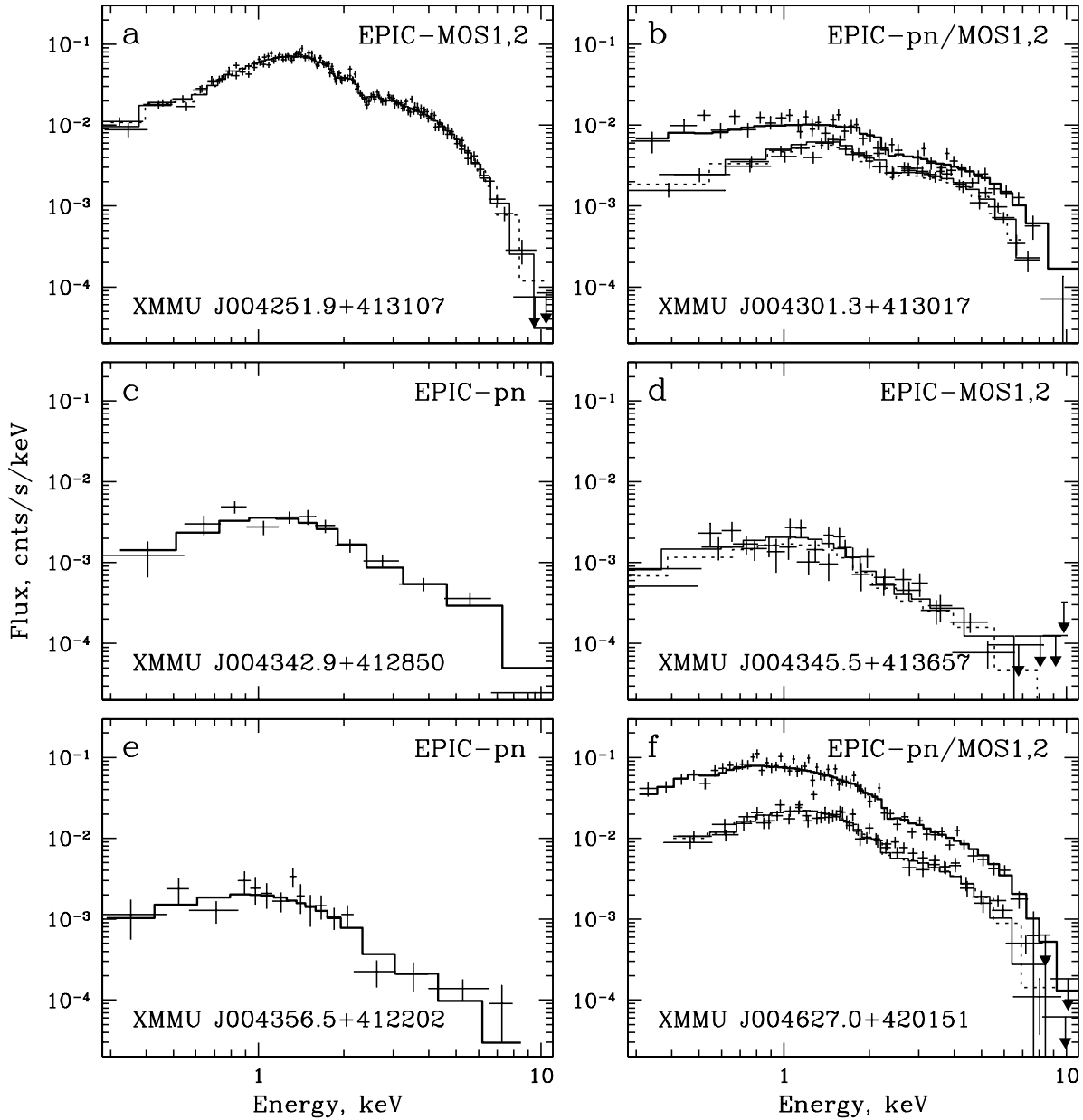


FIG. 6.— *XMM-Newton*/EPIC spectra of the bright X-ray sources coincident with globular cluster candidates (EPIC-pn is always the upper spectrum and the two MOS spectra overlap). Corresponding model fits to the EPIC-pn, MOS1 and MOS2 spectra (Table 4) are shown with thick, thin and dotted histograms respectively. *Panel a*: the X-ray source XMMU J004251.9+413107 (#1), EPIC-MOS1 and MOS2 data (obs. #1), fit by absorbed Comptonization model. *Panel b*: the X-ray source XMMU J004301.3+413017 (#2), EPIC-pn (#4), MOS1 and MOS2 data (obs. #1), fit by absorbed Comptonization model. *Panel c*: the X-ray source XMMU J004342.9+412850 (#4), EPIC-pn data (obs. #1), fit by absorbed simple power law model. *Panel d*: the X-ray source XMMU J004345.5+413657 (#5), EPIC-MOS1 and MOS2 data (obs. #1), fit by absorbed simple power law model. *Panel e*: the X-ray source XMMU J004356.5+412202 (#7), EPIC-pn data (obs. #4), fit by absorbed simple power law model. *Panel f*: the X-ray source XMMU J004627.0+420151 (#27), EPIC-pn, MOS1 and MOS2 data (obs. #2), fit by absorbed Comptonization model.

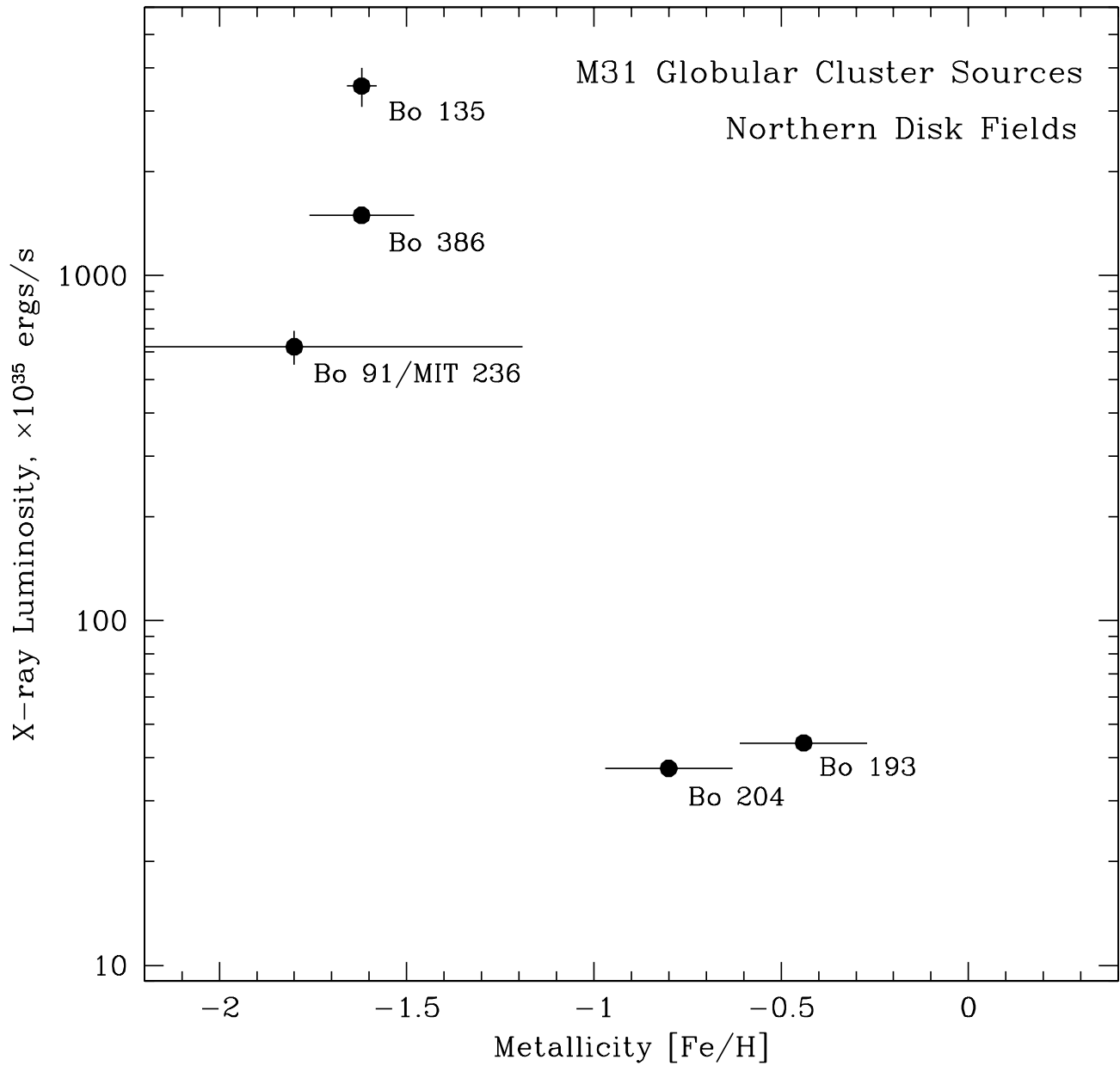


FIG. 7.— The absorbed 0.3 – 10 keV X-ray luminosity of GC sources detected in the *XMM-Newton* observations of the northern disk of M31 vs. metallicity of their host globular clusters. The optical data are from Huchra, Brodie & Kent (1991), Barmby et al. (2000) and Perrett et al. (2002).

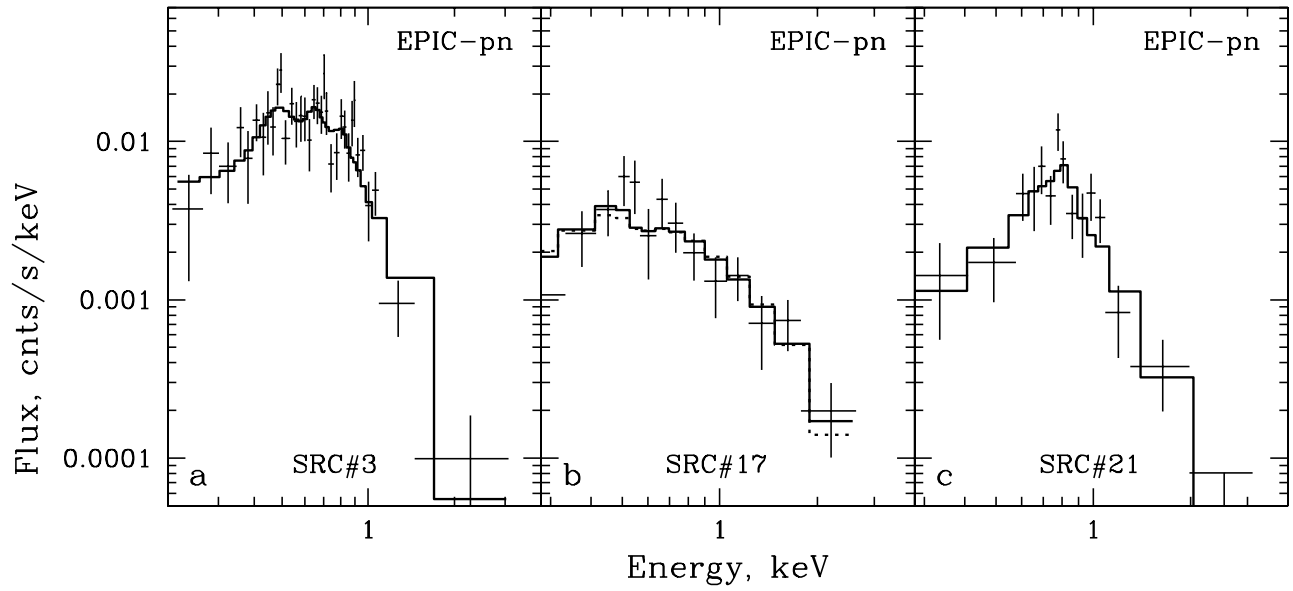


FIG. 8.— EPIC-pn count spectra of three bright SNR candidates: XMMU J004339.1+412654 (*a*), XMMU J004451.1+412907 (*b*) and XMMU J004513.9+413614 (*c*). For each source the best-fit absorbed Raymond-Smith thermal plasma models (RS) are shown with solid histograms. The approximation of the spectrum of XMMU J004451.1+412907 with absorbed simple power law is shown in the *panel b* with dotted histogram.

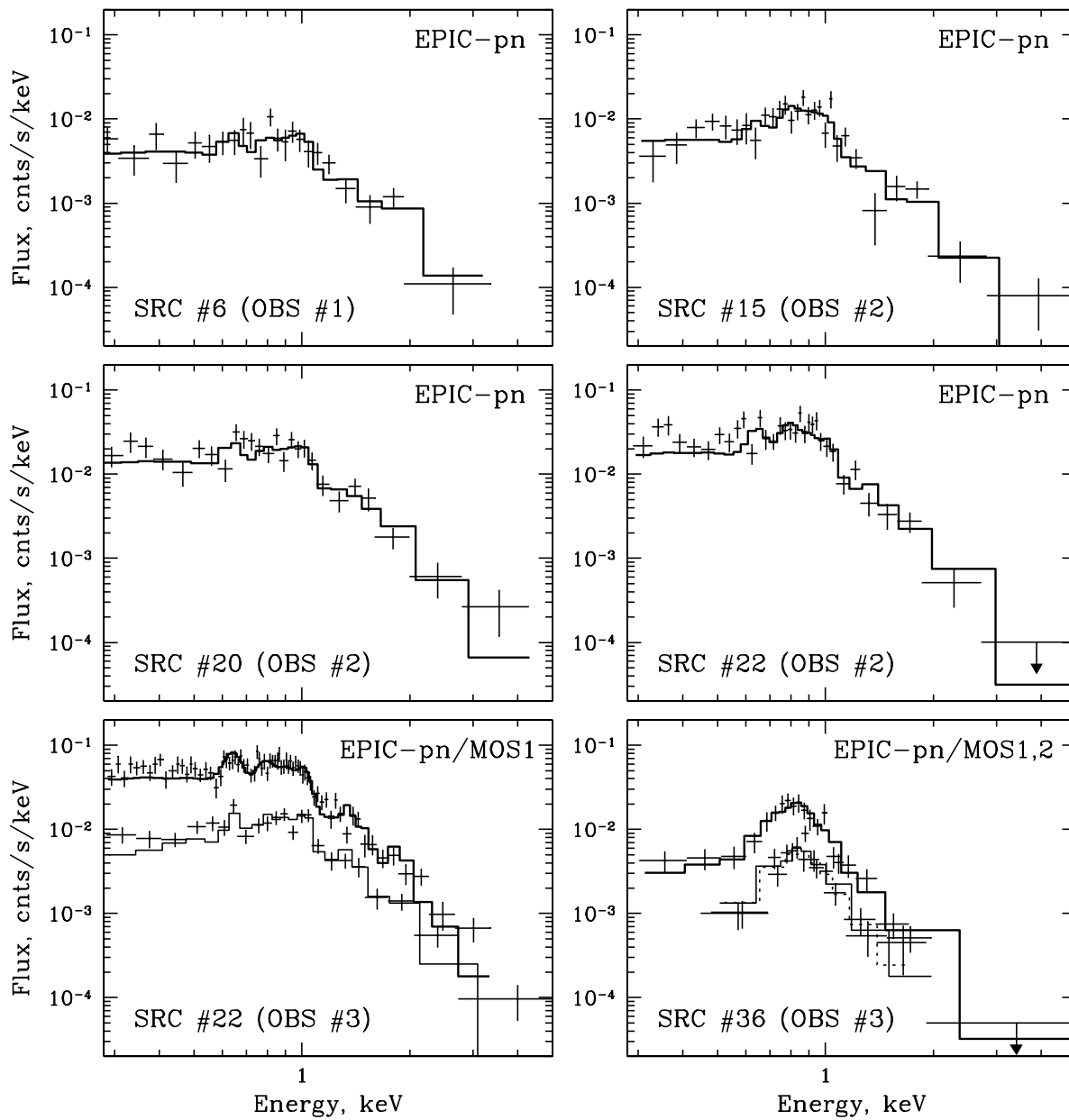


FIG. 9.— EPIC count spectra of Galactic foreground star candidates. The absorbed plasma emission model (RS) fits are shown with thick (EPIC-pn), thin (EPIC-MOS1) and thin dotted (EPIC-MOS2) histograms (pn is always the upper spectrum and the two MOS spectra overlap).

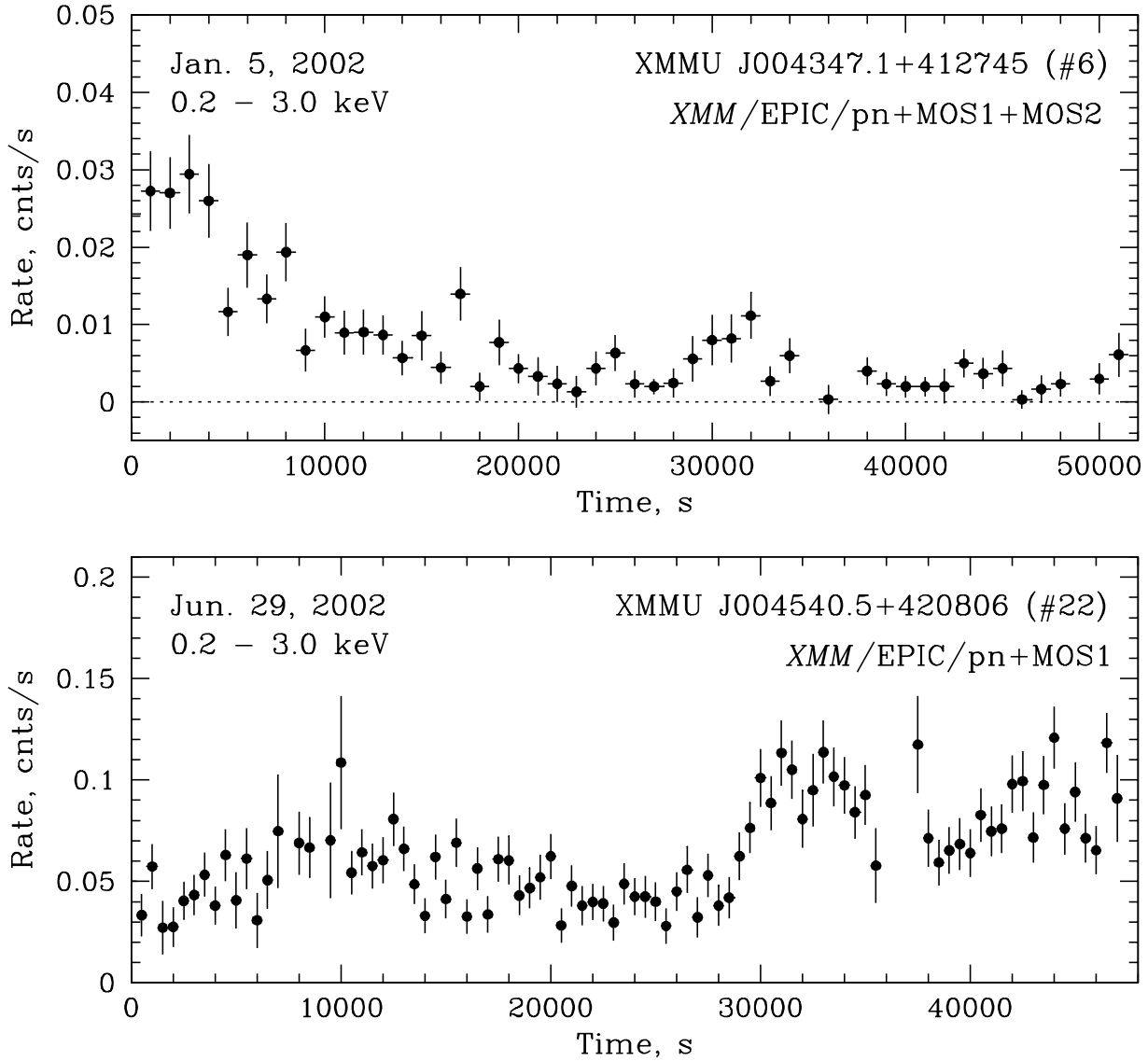


FIG. 10.— *Upper panel:* X-ray light curve of foreground star candidate source XMMU J004347.1+412745 (src #6 in Table 2) during 2002 January 5 *XMM-Newton* observation (Obs. #1), obtained from combined data of EPIC-pn, MOS1 and MOS2 cameras, the 0.2–3.0 keV energy range, and a 1000 s time resolution. *Lower panel:* X-ray light curve of foreground star candidate source XMMU J004540.5+420806 (src #22 in Table 2) during 2002 June 29 *XMM-Newton* observation (Obs. #3), obtained from combined data of EPIC-pn and MOS1 cameras the 0.2–3.0 keV energy range, and a 500 s time resolution.

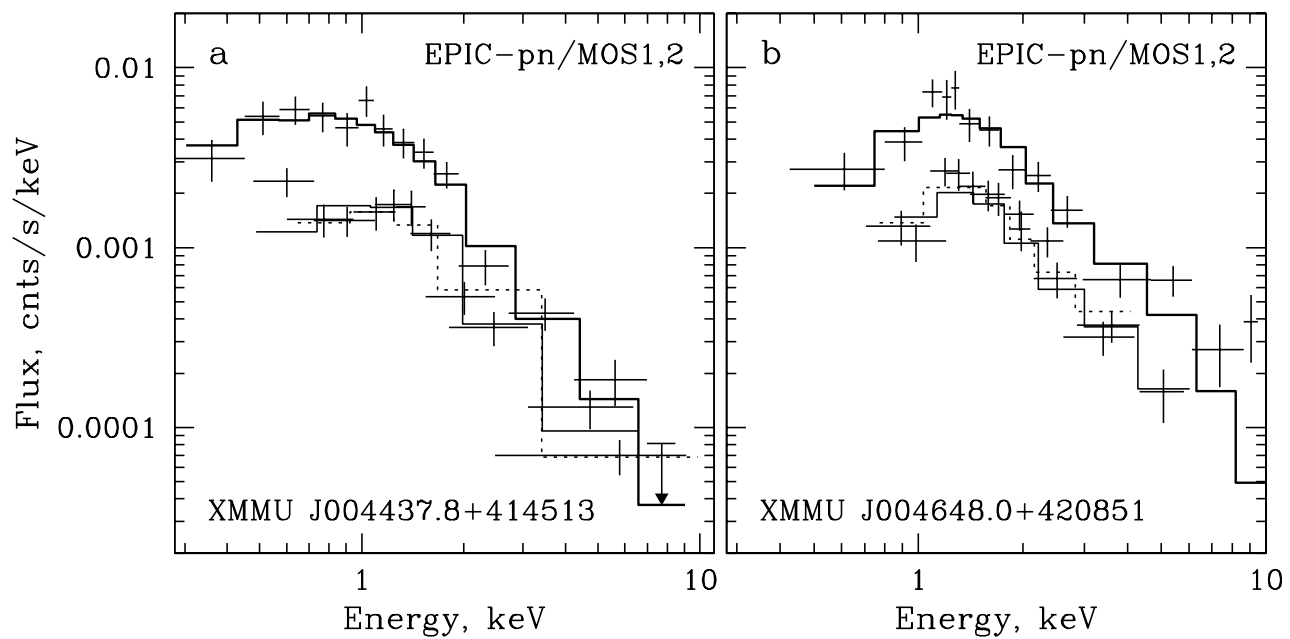


FIG. 11.— EPIC count spectra of two X-ray sources coincident with bright radio sources: XMMU J004437.8+414513 (*a*) and XMMU J004648.0+420851 (*b*). For each source the absorbed power law model best fit to the three EPIC spectra are shown with thick (EPIC-pn), thin (EPIC-MOS1) and thin dotted (EPIC-MOS2) histograms (pn is always the upper spectrum and the two MOS spectra overlap).

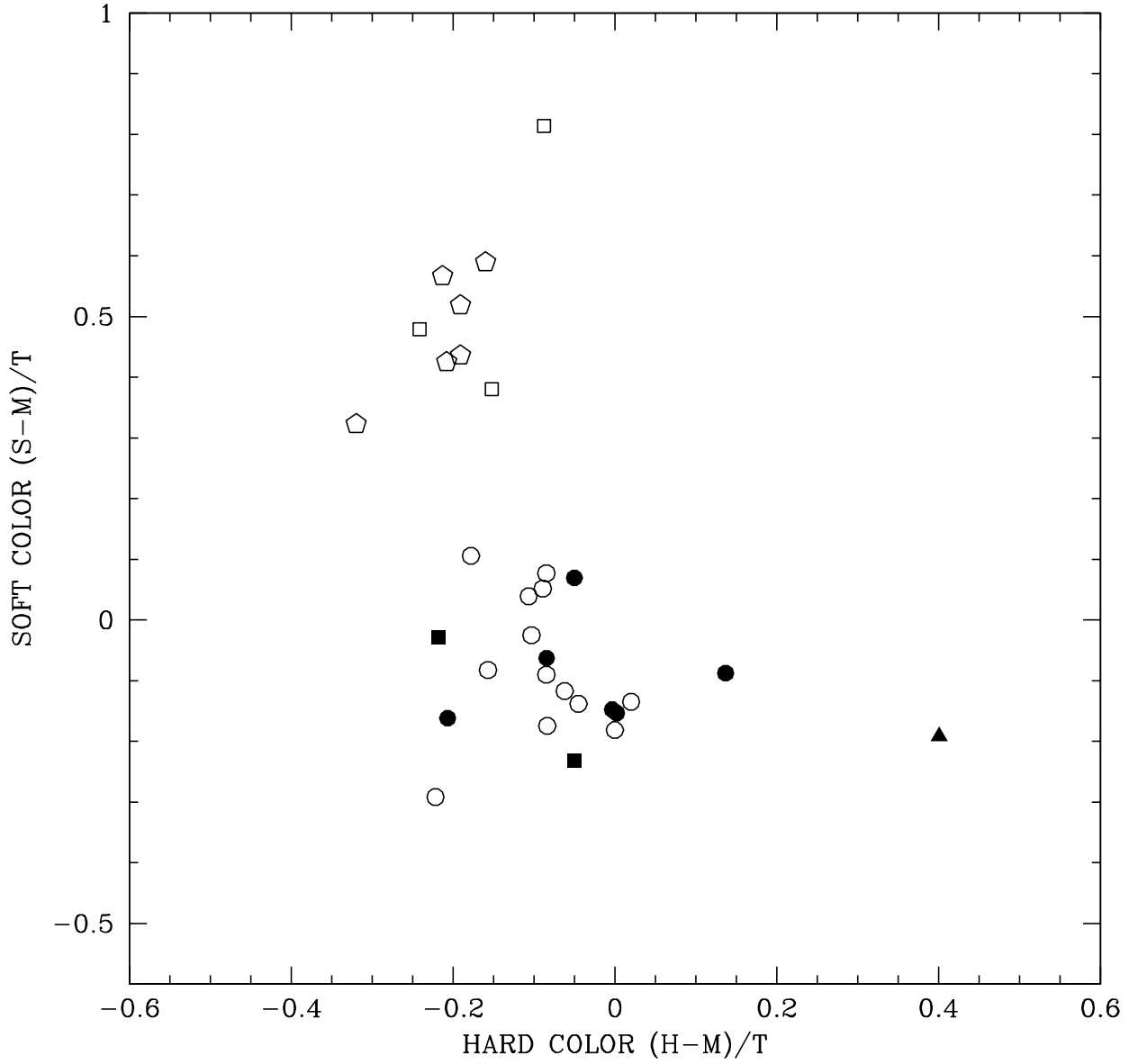


FIG. 12.— X-ray color-color diagram for the bright sources detected with *XMM*/EPIC-pn. The energy bands are: the soft band (0.3 – 1.0 keV), medium band (1.0 – 2.0 keV) and hard band (2.0 – 7.0 keV). Two X-ray colors were defined for each source as: $HR1 = (S - M)/T$ (soft color) and $HR2 = (H - M)/T$ (hard color), where S , M , and H are the counts in soft, medium and hard bands respectively, and T is the total number of source counts in the 0.3 – 7.0 keV energy range. SNR candidates, foreground stars, globular cluster candidates, HMXB pulsar candidate, unidentified sources and radio sources are shown with *open squares*, *filled circles*, *filled triangle*, *open circles*, and *filled squares*.

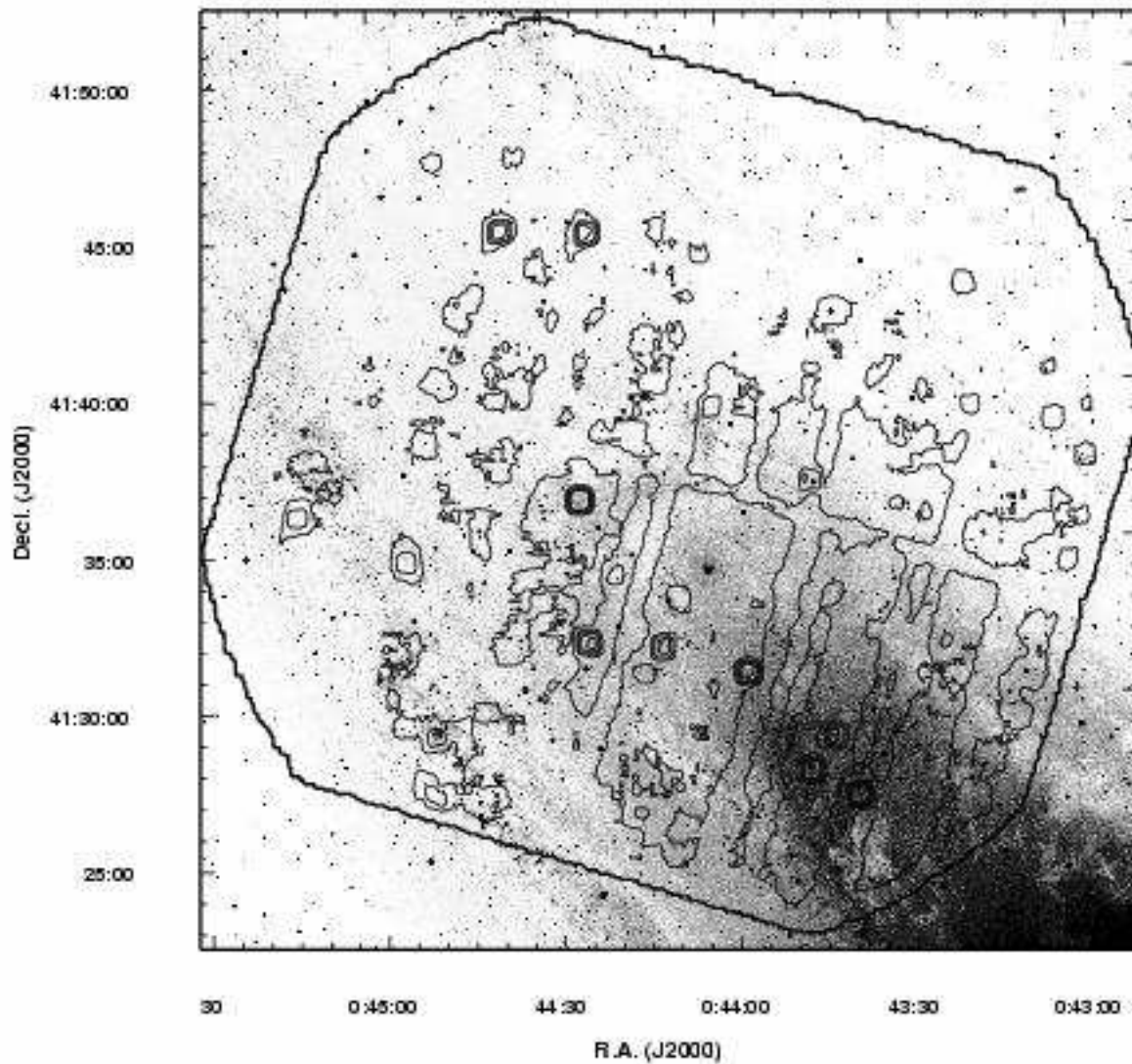


FIG. 13.— Optical image of the northern disk of M31 from the Second Generation Digitized Sky Survey blue plate with *XMM*/EPIC-pn X-ray contours overlaid. X-ray contours were produced using the EPIC-pn image from the Obs. #1 in the 0.2 – 1.5 keV energy band, convolved with circularly symmetric Gaussian function with $\sigma = 20''$. The outer thick contour marks the instrument FOV. The contour levels start at 3.3×10^{-3} cts s^{-1} arcmin $^{-2}$ spaced by equal intervals of 3.3×10^{-3} cts s^{-1} arcmin $^{-2}$. X-ray contours show extended unresolved X-ray emission tracing the structure of the optical disk as well as numerous point-like sources. The cross-like pattern of gaps in contours is due to the gaps between EPIC-pn CCDs and excluded bad detector columns.

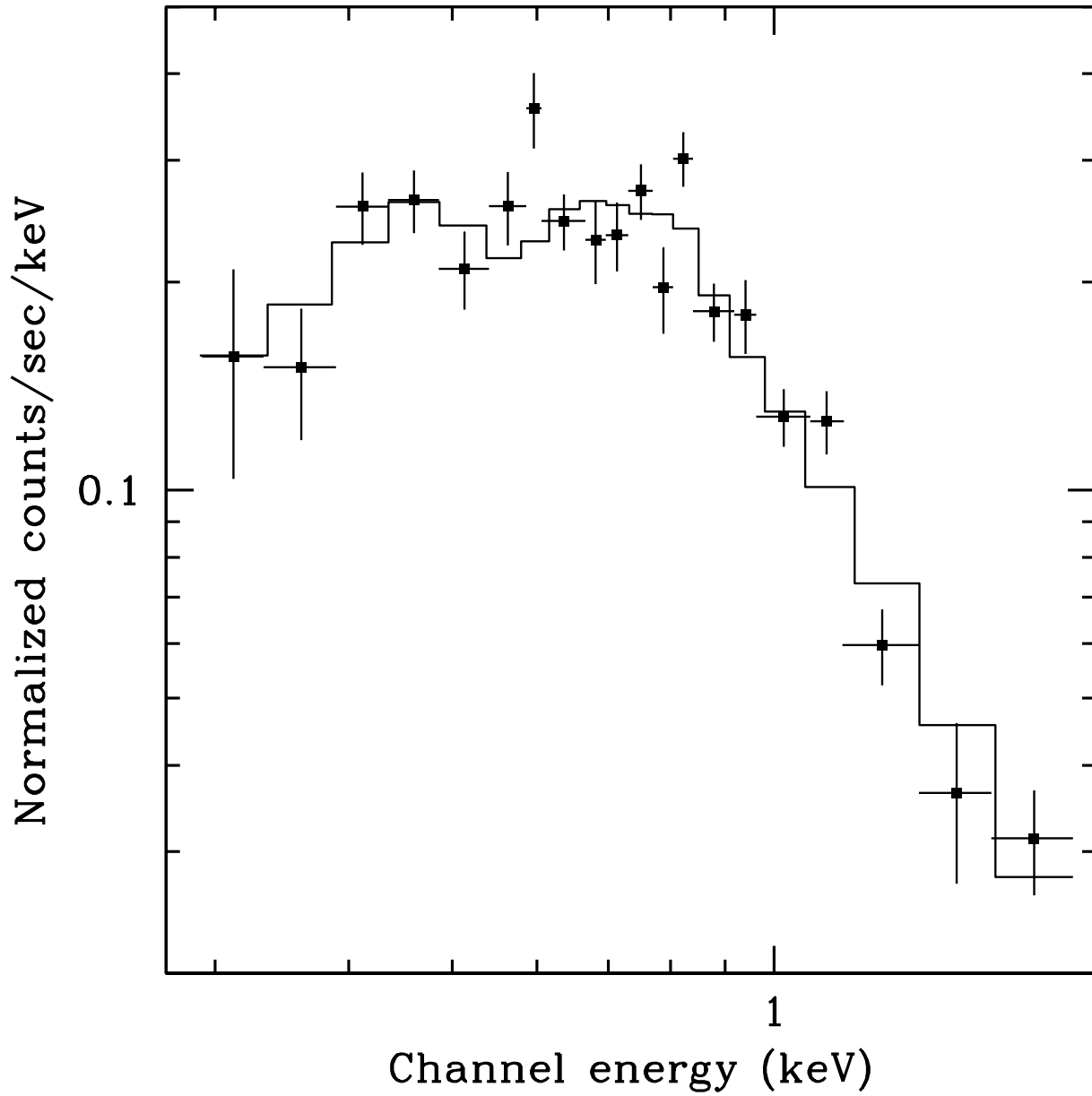


FIG. 14.— Representative EPIC-pn count spectrum of the unresolved X-ray emission from the disk of M31. The approximation with thermal plasma model (RS) is shown with thin histogram.